Thesis for the Degree of Doctor of Philosophy in Physical Chemistry

Structure, phase behavior, and dynamics of colloidal systems characterized by strong, short- and moderate-range attractions:
a computational study

Bodil Ahlström

Department of Chemistry
University of Gothenburg
Sweden

UNIVERSITY OF GOTHENBURG

2010

ISBN 978-91-628-8186-3

Printed by Chalmers Reproservice
Göteborg, Sweden

Abstract

Attractions between colloidal particles are often so strong that non-equilibrium behavior results. However, dissolved non-adsorbing polymer can be added to give a weak attraction between particles so that equilibrium phase transitions appear at moderate polymer concentrations. At higher polymer concentrations and small polymer-colloid size ratios non-equilibrium effects like gelation occur, for which a complete understanding is lacking.
Monte Carlo and Monte Carlo-like computer simulations have been used to investigate the role of many-body effects and the structures that colloidal particles adopt under influence of a polymer-induced depletion attraction. The phase diagram proves difficult to determine for these systems by direct application of the Gibbs ensemble Monte Carlo method, especially for small polymer-colloid size ratios that correspond to short-range attractions. However, a sequential equilibration scheme is shown be able to give equilibrated fluid-fluid coexistence data where usual application of the method fails. The dynamics of colloidal particles along this fluid-fluid coexistence curve is studied by a Brownian dynamics algorithm, corrected for the use of a large time step. The dynamics slows down as the particle and polymer concentrations are increased, but the systems appear to reach equilibrium for the cases studied. This is in contrast to what is found by applying mode coupling theory; it predicts glass-like transitions already at modest polymer concentrations for short-range attractive systems, which is an issue that is investigated to some extent. In addition, a number of approximate theories have been developed and tested against the results from the computer simulations.

List of Papers

This thesis is based upon the following Papers, referred in text by their Roman numerals.

I. **Prediction of structures and gel transitions in systems of colloids with moderate-range attractions**
Bodil Ahlström and Johan Bergenholtz
Journal of Physics: Condensed Matter, **19**, 2007, 036102

II. **Equilibration of fluid-phase coexistence in polydisperse particle systems with short- and moderate-range depletion attractions**
Bodil Ahlström and Johan Bergenholtz
Submitted to Fluid Phase Equilibria

III. **Brownian dynamics of colloidal liquids characterized by short-range depletion interactions**
Bodil Ahlström and Johan Bergenholtz
Manuscript

IV. **Low-density nonergodicity transitions from the idealized mode coupling theory**
Johan Bergenholtz and Bodil Ahlström
Manuscript

Contents

,

Chapter 1

Introduction

Colloidal dispersions are important not only because of their widespread occurrence in everyday items related to food, paint, inks, coatings, and systems found in the pharmaceutical industries, they serve also as important model systems for many biological systems and for the study of fundamental problems in condensed matter science, such as crystallization, gelation, and glass transitions. The phase behavior of colloidal dispersions is of considerable industrial importance but it is also of great fundamental interest. Colloidal particles usually only interact with each other over distances significantly less than the size of the particles. This is particularly the case for attractions [1]. In this sense colloidal attractions can be said to be short ranged compared to those between atoms and molecules. This has a profound influence on the structure, phase behavior, and dynamics of the system, and it is the subject of this thesis. Colloidal particles interacting with short and moderately strong attractions can undergo both equilibrium and non-equilibrium transitions. While the former is well known, an example of the latter is physical gelation. It has been observed experimentally in several, very different colloidal systems and it appears to be a common phenomenon in these types of systems. During the last decade, intensive scientific attention has been given to the gelation phenomenon in attempts to understand the mechanisms behind this process. In spite of this, gelation is far from understood [2]. Clearly, the knowledge of both the microstructural and dynamical behavior as well as the precise characterization of the equilibrium phase diagram is important for investigations of the nature of gel phases. While these processes are sometimes difficult to control precisely in an experiment, computer simulations are characterized by well defined parameters and hence represent an ideal tool to explore the properties of colloidal dispersions. Furhermore, computer simulations bridge the distance between the complexibility of real experiments and the approximate description of theories.

The aim of this thesis is to improve our understanding of the equilibrium and non-equilibrium behavior of colloidal systems of particles interacting via short- and moderate-range attractions. In this process several methods of computer simulation are used and are in many cases optimized for this purpose. Another aim is to to develop, refine, and test some useful theories of structure, phase behavior, and dynamics against results from computer simulations.

We perform a systematic study of the structure, phase behavior, and dynamics of short- and moderate-range attractive systems by use of mainly computer simulations within well-defined model systems. During the course of this study a careful assessment of the model and methology is performed and in Paper I the validity of the model used in the main part of this work, the Asakura-Oosawa-Vrij model [3–5], is examined. Accurate liquid structures within this model are obtained by Monte Carlo simulations and given these liquid structures predictions of the mode coupling theory for the boundary of attractive glass/gel transitions are compared against experimental data. In Paper II the fluid-fluid phase behavior is investigated for a polydisperse version of the same model. It proves difficult to equilibrate the short-range attractive systems of interest in the usual way by Monte Carlo simulations. A sequential equilibration scheme is developed, which enables determining fluid-fluid equilibration data down to reasonably short ranges of attraction. The fluid-fluid phase boundary obtained from this work is used in Paper III as starting point for investigations of the dynamics of the same system. This is done by so-called smart Brownian dynamics simulation, which is shown to be a method that can be used to reach the long time scales necessary to study slow dynamics close to glass transitions. Finally in Paper IV, we return to the mode coupling theory and investigate how it performs for systems with particles interacting via very short-range attractions. In this limit it becomes possible to simplify the theory.

The four scientific papers described above serve as the basis for this thesis. In what follows, I start to provide some background information. In Chapter 2 a general description of colloidal systems, their interactions and phase behavior is given. A description of the models used is given in Chapter 3 and since most of this work is based of computer simulations, I give a summary of the simulation methods used in Chapter 4. In chapter 5 I provide some theoretical background and I also summarize some theoretical models that have been developed as part of this thesis work. The results contained in Papers I-IV are summarized in Chapter 6, and in Chapter 7 some conclusions are given together with suggestions for further work.

Chapter 2

Background

2.1 Colloids

Colloidal systems have been known for a long time and they have been studied systematically since the middle of the 20th century. Colloidal particles are particles within a size range of about one nanometer to some few micrometers, in at least one of their dimensions. These limits are not sharply defined; a colloidal particle should be large enough so that the solvent under most circumstances can be treated as a continuum, i.e. the solvent molecules enter the effective interactions between the colloidal particles only in an averaged way, and so small that it shows thermal motion, commonly referred to as Brownian motion. Brownian motion is relevant only when thermal displacement is a sizeable fraction of the linear dimension of the particle during experimental time ranges. Sedimentation due to gravity provides often a more practical definition of the upper size limit; displacement under the action of gravity should be limited to an extent that allows for experiments on processes for which Brownian motion is relevant. Colloidal dispersions may appear in a variety of ways; they can be aerosols, solid or liquid particles dispersed in a gas, like smoke, fog or hairspray. Solid particles dispersed in a liquid medium are called a dispersion or a sol. Examples of this are printing ink and paint. They can be liquid particles dispersed in a liquid. Such so-called emulsions are, e.g., milk and mayonnaise. Moreover, they can be gas, liquid or solid particles dispersed in solid medium giving rise to solid foam-like structures, solid emulsions like ice cream, and solid dispersions like some alloys. Colloidal dispersions are commonly divided into three classes where the colloidal particles are rigid entities, large flexible macromolecules, or aggregates of small molecules in thermodynamic equilibrium with their environment, like micelles and other self-assembling systems.

To summarize, colloidal dispersions characterize a class of materials that are very common in everyday life. Many industrial products, such as paints, glues, polishes, lubricants, food products, and pharmaceuticals are colloids. Biological materials, like viruses, bacteria, blood, proteins are also colloidal in nature. Colloidal dispersions are also important as model systems. Their characteristic length- and time-scales are such that they allow for direct experimental observations using advanced microscopy techniques down to single-particle resolution and experimental studies in the light scattering regime with fine time resolution. Since the first experiments of Perrin at the beginning of last century [6], colloids have been used as model systems to study fundamental problems of statistical physics, like crystallization, fluid-fluid phase separation, nucleation, and the wetting of solid substrates. Moreover, the properties of colloidal suspensions can often be changed in such a way that both the strength and the range of the interactions can be controlled independently, giving rise to complex and fascinating phase behaviors, with no counterpart in the atomic world [7].

2.2 Colloidal interactions

In a colloidal system, a repulsive interaction due to the size of the partice is always present. Also present are van der Waals forces which originate from the polarizabilities of the atoms building up the colloidal particles. These, often strong, attractions can be minimzed by matching the refractive indices of the particles and solvent molecules. In addition, interactions of electrostatic origin can be present, and additives to the dispersion, like polymers, may influence the interaction between the colloidal particles. In the case of polymers, they can be grafted on the particle surfaces or free in solution. When the polymers are free in solution they may induce a so-called depletion interaction.

Depletion interactions

The colloid-colloid interaction can be changed by adding a second component to the dispersion. Here we consider the case of non-adsorbing polymers. Although these types of interaction can in general be complicated, the focus here is on the case of polymer coils under "theta solvent" conditions where the interactions between the polymers is weak.

Adding a second component, for example a non-adsorbing polymer, to the colloidal dispersion induces an effective interaction between the colloidal particles: a so-called depletion interaction. The depletion interaction is of

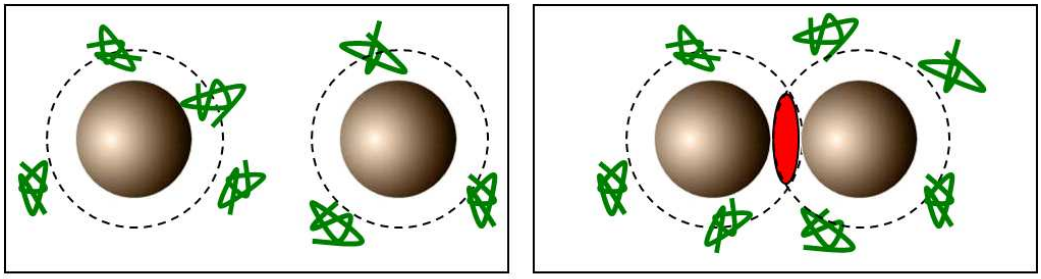

Figure 2.1: Illustration of the depletion interaction. **Left:** The polymer coil (green) center of mass is excluded from a region around the colloidal particle, the depletion zone (dashed line). **Right:** As two colloidal particles approach each other, their depletion zones start to overlap (red region). The polymer coils find more volume available to them and their translational entropy is increased. This increase in entropy leads to an effective attraction between the colloidal particles.

entropic origin. As illustrated in figure 2.1, the polymer coil center of mass is excluded from a region around the colloidal particle, called the depletion zone. When the colloidal particles start to approach each other, their depletion zones overlap and the polymer coils have access to more volume and their translational entropy increases. The increase in entropy can be described by an effective attractive interaction between the colloidal particles even though the particles and polymers may in actuality not exert any attractions on each other at all. This effective attraction can also be viewed as arising from an unbalanced osmotic pressure pushing the colloids together as polymer coils are excluded from the depletion zones between the colloids. By changing polymer concentration and/or polymer molecular weight, the strength and range of the effective attraction can be systematically varied and colloid-polymer mixtures have been developed as an important experimental model system. A particularly simple model for colloid-polymer mixtures was proposed independently by Asakura and Oosawa [3, 4] and by Vrij [5], and it is often referred to as the Asakura-Oosawa (AO) or Asakura-Oosawa-Vrij (AOV) model. In spite of its simplicity, it captures the main features of colloidal-polymer systems. As the AOV model is used in the majority of this work, it will be described in detail in section 3.1.

2.3 Phase behavior

Colloidal systems exhibit a rich and fascinating phase behavior. Also a relatively simple system of spherically isotropic particles show a phase behavior

which depends in a sensitive manner on the interactions characterizing the system. The simplest colloidal system, the hard sphere system, show both equilibrium and non-equilibrium phase transitions [8]. Below the volume fraction $\phi = 0.494$, it is in a fluid state and above $\phi = 0.545$ it freezes completely into a fcc crystal [9]. Between these two volume fractions, the fluid and crystal phases coexist. The equilibrium state above $\phi = 0.545$ is a fully crystalline state up to close packing of $\phi = 0.74$ for fcc crystals. The crystalline state of a hard sphere system is a purely entropic effect; the particles have access to more volume when in a crystal than they would have in a fluid phase at the same volume fraction. Besides these equilibrium transitions also non-equilibrium transitions occur under some conditions. The hard-sphere system shows a glassy state above $\phi \approx 0.58$ [8,10]. In this repulsive glass, the particle dynamics slows down and the system shows solid-like properties but is structurally disordered, like a fluid. This dynamic slowing down and arrest is most often explained by the so-called cage effect [10, 11]. The particles experience themselves as being trapped in a cage made up by their surrounding neighbors. To escape from the cage, which is necessary for behaving like an equilibrium fluid, the cooperative movement of many particles simultaneously is needed. The equilibrium phase behavior is well understood for the hard-sphere system but the glass transition continues to attract scientific attention. When including additional interactions besides the hard-sphere repulsion the situation becomes more complicated.

Adding additional interactions, either repulsive, attractive, or a combination of both, complicates the phase behavior. In this work the focus is on systems composed of spherical hard-core particles with an additional short- or moderate-ranged attraction. If the range and strength of attraction is large enough the colloidal fluid can phase separate into a low-density, i.e. dilute, colloid fluid and a higher-density colloidal fluid, similar in some ways to the gas-liquid transition in the atomic case. At higher particle concentrations the freezing transition occurs. So far, the phase diagram is similar to that of an atomic system; it has a critical point and a triple point. This is the situation illustrated in the left part of figure 2.2. The phase behavior of the attractive system depends sensitively on the range of attraction [12–14]. Decreasing the range of attraction, the critical point drops because stronger attractions are needed for phase separation to compensate for the shorter range. Eventually the fluid-fluid coexistence line or binodal becomes metastable with respect to crystallization. For a suffiently short-ranged attractive system, the thermodynamic equilibrium state is either a low-density fluid, a crystal phase, or both in equilibrium with each other, as illustrated in the right part of figure 2.2, where also the metastable fluid-fluid binodal (solid line) is shown. The critical point becomes metastable when the range of attrac-

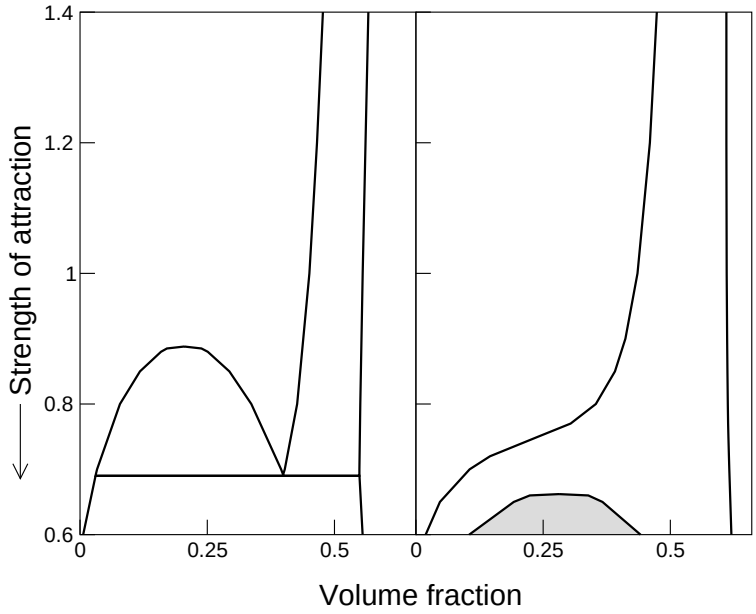

Figure 2.2: Schematic equilibrium phase diagram in terms of strength of attraction and volume fraction for systems characterized by attractive interactions. **Left:** Here the attraction is of longer range relative to the particle size. The system exhibits fluid-fluid phase separation and it has a critical point and a triple point. **Right:** For sufficiently short-range attractions, the fluid-fluid binodal is metastable with respect to crystallization and the critical and triple points are absent.

tion is lower than about 15 % of the particle diameter if one replaces the interaction by an effective square-well potential [15]. The equilibrium crystal phase is a fcc crystal, but Bolhuis and Frenkel [16] have predicted that for very short-ranged attractions also a crystal-crystal phase transition occurs at high densities.

Also the attractive systems show non-equilibrium transitions. At high densities and low attraction strength, the situation is similar as that for the hard-sphere model – a repulsive glass is formed. At these high densities it has been found that by increasing the attraction strength a melting of the repulsive glass takes place, which means equilibrium is recovered by adding a weak attraction. The interpretation is that a weak clustering of the spheres opens up the cage and the particles may more easily escape and the glass melts [17]. Increasing the attraction strength further, the attractions become strong enough for the particles to "bond" physically to each other and an attraction-driven glass is formed [17–21]. For systems with short-range attractions, glass-like transitions occur also at lower volume fractions [22],

where they are commonly referred to as gels or physical gels because the bonds between the particles are non-covalent. Colloidal gels are being studied quite intensely and it seems that they are created during the interplay between fluid-fluid phase separation and some form of structural arrest [2,23]. There is some indication that this structural arrest may come from the attractive glass regime which many times comes in close proximity to the fluid-fluid binodal.

For these types of systems the equilibrium phase behavior is reasonably well understood, albeit not easily predicted with quantitative accuracy theoretically or determined by computer simulations. Polydispersity in particle size complicates matters and only some qualitative trends are known. Even less is known of the effects of polydispersity on glass and gel transitions. It is known that phase separation of polydisperse systems is associated with fractionation to varying degree, such that the coexisting phases not only differ in volume fraction from the 'parent' system but also in composition. This effect requires consideration in studies of colloidal phase behavior because colloidal systems are almost invariably polydisperse to some degree.

Chapter 3

The Model

Colloidal dispersions are complex fluids, and the theoretical treatment of them usually has to rely on coarse-graining techniques. Due to the large time- and length-scale differences between the colloidal particles and the solvent molecules in the dispersion, the solvent can under most circumstances be treated as a continuum. The solvent degrees of freedom are integrated out, and the resulting effective interaction energy between the colloidal particles is a free energy, a potential of mean force, $U(\mathbf{r}^N)$. Generally, $U(\mathbf{r}^N)$, is complicated and depends on the coordinates of all N particles. Usually pair-wise additivity is assumed, i.e. the interaction potential is expressed as a sum over pair-potentials, which for spherically symmetric particles is:

$$U(\mathbf{r}^N) = \frac{1}{2}\sum_{i}^{N}\sum_{j\neq i}^{N} u(\mid \mathbf{r}_i - \mathbf{r}_j \mid) \tag{3.1}$$

Pair-wise additive model potentials have been shown to give results in good agreement with experimental data in many cases. Within the Asakura-Oosawa-Vrij model used in this work, the assumption of pair-wise additivity is exact for polymer-colloid size ratios smaller than about 0.1547 [12, 24] and we have shown in Paper I that pair-wise additivity is a good approximation also for the case of the somewhat larger size ratios used in our work.

3.1 The Asakura-Oosawa-Vrij model

The Asakura-Oosawa-Vrij (AOV) model was proposed already in the 1950's by Asakura and Oosawa [3, 4] and later also independently by Vrij [5]. The AOV model aims to describe the depletion interactions present in a system of hard-sphere colloids dispersed in a polymer solution at near-theta conditions.

The model can be described in two, under some circumstances, equivalent ways. In Vrij's formulation of the model, it is described as a non-additive binary hard-sphere mixture [5,25]. The colloids are modeled as hard spheres whereas the polymers are treated as an ideal gas, i.e. they are freely able to penetrate one another, but with a hard-sphere interaction with respect to the colloids, i.e.

$$u_{cc}(r) = \begin{cases} \infty & r < \sigma_c \\ 0 & r > \sigma_c \end{cases} \tag{3.2}$$

$$u_{cp}(r) = \begin{cases} \infty & r < \sigma_{cp} \\ 0 & r > \sigma_{cp} \end{cases} \tag{3.3}$$

$$u_{pp}(r) = 0 \tag{3.4}$$

Here, r is the center-to-center separation distance, σ is the particle diameter, the subscripts c and p denote colloids and polymers, respectively, and $\sigma_{cp} = (\sigma_c + \sigma_p)/2$.

Alternatively, the system can be described as an effective one-component system in which the colloidal particles interact in a pair-wise additive manner; they possess a hard-core repulsion preventing overlap plus an attractive interaction, given by the so-called Asakura-Oosawa (AO) potential:

$$\beta u_{AO}(r) = -\phi_p^{(R)}(1+\xi)^3 \left[1 - \frac{3}{2}\left(\frac{r/\sigma_c}{1+\xi}\right) + \frac{1}{2}\left(\frac{r/\sigma_c}{1+\xi}\right)^3\right] \tag{3.5}$$

The size ratio, $\xi = \sigma_p/\sigma_c$, determines the range of the attraction and the volume fraction of the polymer $\phi_p^{(R)}$ sets the magnitude of the attraction. Actually it is the osmotic pressure of the polymer solution that determines the magnitude of the attraction so it is more correct to state that it is the number density of polymer, viz. $\Pi = n_p^{(R)} k_B T$, that to leading order accounts for the well depth. Also it is important that the volume fraction be based on the volume available to the polymers as indicated by the superscript [13,22].

For small size ratios, $\xi \leq 2/\sqrt{3} - 1 \approx 0.1547$, all three- and higher body contributions to the effective potential vanish [12] and these two descriptions become equivalent provided the mapping between them is done in a self-consistent way [24]. The key parameter in this context is the free-volume fraction $\alpha = \phi_p/\phi_p^{(R)}$ of such an idealized colloid-polymer mixture, relating the polymer volume fractions ϕ_p and $\phi_p^{(R)}$ to one another. The free-volume fraction depends not only on the volume fractions but also implicitly on the colloid structure as [24]:

$$\alpha = \frac{\phi_p}{\phi_p^{(R)}} = 1 - \phi_c\,(1+\xi)^3 - \frac{12\phi_c^2\xi^3}{\phi_p^{(R)}} \int_1^{1+\xi} dr r^2 g_{cc}(r;\phi_c,\phi_p^{(R)})\beta u_{AO}(r) \tag{3.6}$$

Here, r has been made non-dimensional with σ_c, and $g_{cc}(r;\phi_c,\phi_p^{(R)})$, the colloid-colloid radial distribution function, is obtained from a system of colloids interacting via the AO-potential in equation 3.5.

The AO potential, extended to take polydispersity into account, for two spheres i and j with diameters σ_i and σ_j, respectively, in the presence of monodisperse polymer with diameter σ_p is given by [26]:

$$\beta u(z) = -\phi_p^{(R)}\Big\{ (1+\overline{\eta})^3 - \frac{3}{2}z\,(1+\overline{\eta})^2 + \frac{1}{2}z^3 - \frac{3}{8}\frac{1}{z}\,(\eta_i-\eta_j)^2\,[z-(1+\overline{\eta})]^2]\Big\} \tag{3.7}$$

where z is the distance between particles i and j normalized with the polymer diameter, $z=\frac{r_{ij}}{\sigma_p}$, and $\eta_i=\frac{\sigma_i}{\sigma_p}$, and $\overline{\eta}=\frac{1}{2}\,(\eta_i+\eta_j)$. The polydispersity causes differences in the interaction between different pairs of particles. Apart from the differences in the hard-core interaction resulting from the differences in particle diameters the attractive well depth also increases with particle size.

In spite of its simplicity, the effective AO pair potential is known to capture the main features of polymer-colloid mixtures. The fully tunable character, both in terms of magnitude and range of the attraction, of the AO-potential makes it not only interesting from a theory and simulation point of view, but colloid-polymer systems have become established as the experimental model systems of choice for systematic studies of, e.g., structure, dynamics, and phase behavior [7].

3.2 Square well potential

Another commonly used model system for describing colloidal systems is the square well (SW) model. The SW potential is given by a hard core repulsion and an adjacent attraction in the form of a well.

$$u(r) = \begin{cases} \infty & 0<r<\sigma \\ -\epsilon & \sigma<r<\lambda\sigma \\ 0 & \lambda\sigma<r \end{cases} \tag{3.8}$$

where ϵ is the well depth, $\lambda=1+\delta$, characterizes the range over which the attraction acts, and r is the center-center distance of separation.

3.3 Schulz distribution

Colloidal dispersions are with some exceptions known to exhibit a size distribution, a shape distribution and in the case of charged particles also a charge distribution. While the shape distribution often can be avoided, it

is harder to completely reduce the size- and charge distributions. The size polydispersity of many colloidal systems is known to be modeled well by the Schulz distribution [27, 28], which is given by:

$$f(\sigma) = \left(\frac{z+1}{\overline{\sigma}}\right)^{z+1} \frac{\sigma^z}{\Gamma(z+1)}\, e^{(z+1)\frac{\sigma}{\overline{\sigma}}} \tag{3.9}$$

where σ is the particle diameter, $\Gamma(z)$ is the gamma function and z is a parameter controlling the width (polydispersity) of the distribution.

In a computer simulation of a finite number of particles, it is appropriate to work with a discrete representation of the continuous Schulz distribution. Following the methology developed by D'Aguanno and Klein [29], it is possible to approximate the continuous distribution by a discrete N-component mixture by requiring equality of moments. Working with normalized moments:

$$\sum_{i=1}^{M} x_i = \int_0^\infty d\sigma f(\sigma) = 1 \tag{3.10}$$

$$\sum_{i=1}^{M} x_i \frac{\sigma_i}{\bar{\sigma}} = \bar{\sigma}^{-1} \int_0^\infty d\sigma \sigma f(\sigma) = 1 \tag{3.11}$$

$$\sum_{i=1}^{M} x_i \left(\frac{\sigma_i}{\bar{\sigma}}\right)^2 = \bar{\sigma}^{-2} \int_0^\infty d\sigma \sigma^2 f(\sigma) = \frac{z+2}{z+1} \tag{3.12}$$

$$\sum_{i=1}^{M} x_i \left(\frac{\sigma_i}{\bar{\sigma}}\right)^3 = \bar{\sigma}^{-3} \int_0^\infty d\sigma \sigma^3 f(\sigma) = \frac{(z+3)(z+2)}{(z+1)^2} \tag{3.13}$$

and so on. Here, x_i is the mole fraction of particles belonging to component i with diameter σ_i.

Already a small number of components in the mixture give quantitative results for many applications. In the approach by D'Aguanno and Klein a discrete M-component representation of the continuous Schulz distribution is obtained by matching the first $2M$ moments and solving equations like 3.10-3.12 for M mole fractions and M diameters. In a computer simulation we require integer numbers of particles and therefore only the first M moments can be enforced, whereby M equations are solved for the diameters for a set of prescribed mole fractions. For a ternary mixture only equations 3.11 - 3.13 have to be solved for the three diameters given appropriate mole fractions.

Chapter 4

Computer simulations

Computer simulations have, all since computers became available for non-military use in the early 1950s, developed as an increasingly important tool in a variety of scientific areas. The reasons for their importance are numerous. They can be ethical; for example, the use of animal experiments and chemicals affecting the environment can be minimized by replacing experiments with computer simulations. Computer simulations are accessible where real world experiments are difficult or even impossible to perform. They can be done under conditions of extreme temperatures and pressures or under conditions inappropriate for reasons like hazardness. They can also be used to investigate materials which are very rare or which have not been prepared yet and they are often cost effective. In computer simulations, the microstructure of a material is easily obtained, i.e. the detailed information of the positions of all particles are available. This information, which is important for the fundamental understanding of how and why different processes occur, is often difficult to determine experimentally. Computer simulations are also important for the development of theories. Theories are invariably approximate to varying degree. As computer simulations provide an exact result within a given model, they serve as critical tests for approximate theories. In this work, we have used mainly Monte Carlo or Monte Carlo-like computer simulations to investigate both microstructures, phase behavior, and dynamics of colloidal systems and to test theories.

4.1 Monte Carlo simulations

The name Monte Carlo simulation originates from the heavy use of computer generated random numbers by the method. The Monte Carlo (MC) simulation method relies on statistical mechanics and can be performed in a variety

of ensembles. In what follows, a brief description of the methods used in this work, canonical MC, Gibbs ensemble Monte Carlo (GEMC), and a so-called smart Brownian dynamics method, is given. [30]

4.1.1 Canonical Monte Carlo

In a Monte Carlo simulation in the canonical ensemble, i.e. a simulation of a system with fixed number of particles (N), in a given volume (V), and at a given temperature (T), the classical partition function for N identical particles reads as

$$Q_{NVT} = \frac{1}{h^{3N}N!}\int d\mathbf{p}^N d\mathbf{r}^N e^{-\beta H(\mathbf{p}^N,\mathbf{r}^N)} \tag{4.1}$$

where the Hamiltonian (H) is the sum of the kinetic (K) and the potential (U) energies, $H = K + U$, of the system. $\mathbf{r}^N$ and $\mathbf{p}^N$ are the coordinates and the momenta, respectively, of all N particles. Integrating over the momenta, $\mathbf{p}^N$, gives

$$Q_{NVT} = \frac{1}{N!\lambda^{3N}}Z_{NVT} \tag{4.2}$$

where λ is the thermal de Broglie wavelength and Z is the configurational partition function:

$$Z_{NVT} = \int d\mathbf{r}^N e^{-\beta U(\mathbf{r}^N)} \tag{4.3}$$

While in experiments time averages for a given quantity usually are determined, the corresponding averages calculated in Monte Carlo simulations are ensemble averages. The so-called *ergodic hypothesis* states that, provided all configurations can be realized in a finite amount of time, the time and ensemble averages are identical. An ensemble average of a phase function $A(\mathbf{p}^N, \mathbf{r}^N)$ is defined as:

$$\langle A\rangle = \frac{\int d\mathbf{p}^N d\mathbf{r}^N e^{-\beta H(\mathbf{p}^N,\mathbf{r}^N)} A(\mathbf{p}^N,\mathbf{r}^N)}{Q_{NVT}} \tag{4.4}$$

and the probability density, P, of finding the system at the phase point $(\mathbf{p}^N, \mathbf{r}^N)$ equals

$$P = \frac{e^{-\beta H(\mathbf{p}^N,\mathbf{r}^N)}}{Q_{NVT}} \tag{4.5}$$

When the function A has a simple dependence on the momenta it can be integrated over analytically and we can focus on the configurational part, given by the configurational ensemble average

$$\langle A\rangle = \frac{\int d\mathbf{r}^N e^{-\beta U(\mathbf{r}^N)} A(\mathbf{r}^N)}{Z_{NVT}} \tag{4.6}$$

and later one can add the contribution from the momentum-dependent part. The configurational probability density function, ρ_{NVT}

$$\rho_{NVT} = \frac{e^{-\beta U(\mathbf{r}^N)}}{Z_{NVT}} \tag{4.7}$$

is the probability to find the system in configuration $\mathbf{r}^N$ irrespective of the momenta. Numerical integration requires descretizing using L points along each of the $3N$ coordinates; the integrand has thus to be evaluated L^{3N} times for each configuration. Also, the probability of realizing any configuration is proportional to the strongly varying Boltzmann factor $e^{-\beta U}$ and numerical integration schemes usually works best for functions that are smooth over distances corresponding to the mesh size. Clearly, numerical integration of these types of integrals is impossible for real systems. Moreover, integrating the integrand in for example a dense liquid, the Boltzmann factor is vanishingly small for the overwhelming majority of phase points. It would be preferable to sample many points along the trajectory where the Boltzmann factor is large and a few elsewhere. This is the principal idea of importance sampling. In general, it is not possible to evaluate an integral such as in equation 4.3 by direct Monte Carlo importance sampling. However, in many cases, it is not the integral itself which is interesting but averages of the type in equation 4.6. Hence, it is the ratio of two integrals which has to be evaluated. Metropolis *et.al.* [31] devised a scheme to sample such a ratio by construction of an importance-weighted random walk in configuration space, generating points in configurational space with a probability density proportional to the Boltzmann factor.

In the NVT-Monte Carlo method, where a system with N particles in a constant volume V and at temperature T is simulated, this is achieved by displacement of the N particles according to certain acceptance criteria. The acceptance rules are chosen such that these configurations occur with a frequency prescribed with the desired probability distribution, the Boltzmann distribution.

MC simulations of a fluid system aim to provide information about the properties of a macroscopic sample. Due to computer limitations, most simulations probe the structural and thermodynamical properties of a system of a few hundreds to a few thousands of particles or perhaps tens of thousands on some occasions. Clearly, this number is far from the thermodynamic limit. In order to simulate bulk phases it is essential to choose boundary conditions that mimic the presence of an infinite bulk surrounding the N-particle model system. This is usually done by employing periodic boundary conditions (PBC). The use of PBC proves to be an effective method to simulate

homogeneous bulk systems, at least away from a continuous phase transition, where problems, mainly due to density fluctuations and a growing correlation length, with PBCs can be expected.

4.1.2 Gibbs ensemble Monte Carlo

NVT-MC is not the proper choice of method to determine coexistence curves, at least not if a system with a moderate number of particles is simulated. If two phases coexist in such systems, a relative large fraction of all particles reside in or near the interface between the phases. This is a non-negligible effect even for quite large systems. A relatively important free-energy cost is associated with the creation of an interface, so much so that, for sufficiently small systems, it is favorable for the system not to phase separate at all [30]. There exist several schemes to study phase coexistence without creating an interface. For fluids, a well known method is the Gibbs ensemble Monte Carlo (GEMC) method.

With the GEMC method by Panagiotopoulos [32], phase equilibria can be studied in a single simulation. In the GEMC method, where phase equilibrium is simulated under conditions where the pressure, temperature and chemical potential(s) of the coexisting phases are equal, the system spontaneously finds the densities and compositions of the coexisting phases. Here, focus is on the version of the GEMC method were the total number of particles and the total volume of the two boxes remains constant, i.e. at constant N, V, T conditions.

The partition function for N particles distributed over the two volumes V_1 and V_2 and at temperature T is [33]

$$\begin{aligned} Q_G(N,V,T) \equiv & \sum_{n_1=0}^{N} \frac{1}{V\lambda^{3N} n_1!(N-n_1)!} \int_0^V dV_1 V_1^{n_1} (V-V_1)^{N-n_1} \\ & \int d\mathbf{s}_1^{n_1} e^{-\beta U(\mathbf{s}_1^{n_1})} \int d\mathbf{s}_2^{N-n_1} e^{-\beta U(\mathbf{s}_2^{N-n_1})} \end{aligned} \tag{4.8}$$

where, again, λ is the thermal de Broglie wavelength. $\mathbf{s}_i$ is the coordinates for all particles in box i, scaled with the box length, i.e. $\mathbf{s}_i^{n_i} = r_i^{n_i}/L_i$. The indices indicate the box association. The two volumes, V_1 and V_2, can change in such a way that the total volume, $V = V_1 + V_2$, remains constant. It follows that the probability of finding a configuration with n_1 particles in box 1 with volume V_1 and positions $\mathbf{s}_1^{n_1}$ and $\mathbf{s}_2^{N-n_1}$ is given by:

$$P(n_1, V_1, \mathbf{s}_1^{n_1}, \mathbf{s}_2^{N-n_1}) \propto \frac{V_1^{n_1}(V-V_1)^{N-n_1}}{n_1!(N-n_1)!} e^{-\beta[U(\mathbf{s}_1^{n_1})+U(\mathbf{s}_2^{N-n_1})]} \tag{4.9}$$

From equation 4.9 it follows that, to sample all possible configurations of two subsystems which can exchange particles and volume, three types of moves are needed: displacements of particles, changes of volume under the condition that the total volume is unchanged, and transfer of particles between the two boxes. Depending on how the moves are constructed, the acceptance criterion is adjusted so that the desired probability distribution is obtained.

The GE method is known to perform well for determination of phase transitions, at least away from the closest vicinity of the critical point. Its main limitation is that it breaks down when at least one of the two phases become so dense that it becomes impossible to exchange particles effectively. Moreover, it is possible to determine the chemical potential in either box directly from the particle exchange move via an insertion formula [33]

$$\mu^a = -k_B T ln \left\{ \lambda^{-3} \left\langle \frac{V^a}{N^a + 1} e^{-\beta U^a +} \right\rangle \right\} \tag{4.10}$$

where $U+$ is the energy change that results from inserting a particle in box a, and μ^a, V^a, and N^a are the chemical potential, volume, and number of particles in box a.

4.2 Smart Brownian dynamics

The Brownian Dynamics (BD) simulation method is a technique used to simulate the dynamics of particles that undergoes Brownian motion. This technique takes advantage of the fact that it is a large time and length scale difference between the Brownian particles and the solvent molecules. The dynamics of the coarse-grained system, neglecting hydrodynamic interactions, can be described by the Langevin equation:

$$\mathbf{F}_i^{tot}(t) = \mathbf{F}_i^{int}(t) + \mathbf{F}_i^{F}(t) + \mathbf{F}_i^{B}(t) \tag{4.11}$$

The total force on particle i is expressed as a sum of the net interaction force between the particle i and the other Brownian particles, the force which derives from the potential of mean force $\mathbf{F}_i^{int}(t)$, and the forces due to interactions between the particle and the solvent molecules. Treating the solvent as a continuum, the systematic collisions with the solvent molecules are described by a determinisic friction force, $\mathbf{F}_i^{F}(t) = \zeta \dot{\mathbf{r}}_i(t)$, and a stochastic force $\mathbf{F}_i^{B}(t)$ which aims to mimic the random collisions of the solvent molecules and the Brownian particle. Here, ζ is Stokes' friction coefficient, $\mathbf{F}_i^{B}(t)$ is Gaussian-distributed with $\langle \mathbf{F}_i^{B}(t) \rangle = 0$ and $\langle \mathbf{F}_i^{B}(t) \mathbf{F}_j^{B}(t') \rangle = 2 k_B T \zeta \delta_{ij} (t - t')$.

Averaging the Langevin equation over a time interval Δt large compared to the solvent time scale, the particle accelerating term in the above momentum Langevin equation can be neglected,

$$m\ddot{\mathbf{r}}_i(t) = \mathbf{F}_i^{int}(t) - \zeta\dot{\mathbf{r}}_i(t) + \mathbf{F}_i^{B}(t) \approx 0 \tag{4.12}$$

and using the Stokes-Einstein relation, the positional Langevin equation can be written as:

$$\dot{\mathbf{r}}_i(t) = \beta D_{0,i}\mathbf{F}_i^{int}(t) + \beta D_{0,i}\mathbf{F}_i^{B}(t) \tag{4.13}$$

The Brownian Dynamics simulation is performed by integrating this stochastic differential equation forward in time by an appropriate algorithm. A commonly used algorithm is the Ermak scheme [34]:

$$\mathbf{r}_i(t_0+\tau) = \mathbf{r}_i(t_0) + \beta D_{0,i}\mathbf{F}_i^{int}(t_0)\tau + \sqrt{2D_{0,i}\tau}\mathbf{n} \tag{4.14}$$

where τ is the time step and $\mathbf{n}$ is a vector of independent Gaussion-distributed random numbers with zero mean and unit variance.

The standard Brownian Dynamics method employing the Ermak scheme requires finite and continuous forces. Since the Asakura Oosawa model system used in this work includes a hard-sphere repulsive potential we have chosen to use so-called Smart Brownian Dynamics [35–39], a method designed to deal with hard-sphere interactions and other steep repulsive interactions. It is a force-bias MC method in which the Ermak scheme is used to generate the trial displacements of the particles. The moves from the old state (o) to the new state (n) are then accepted with a probability $min(1, P_{o\to n})$, where $P_{o\to n}$ is:

$$\begin{aligned} P_{o\to n} = \; & exp\Big[-\beta(U_n - U_o) - \tfrac{1}{2}(\mathbf{r}_i^n - \mathbf{r}_i^o)\beta(\mathbf{F}_i^n - \mathbf{F}_i^o) - \\ & \tfrac{1}{4}D_{0,i}\tau\beta^2(\mathbf{F}_i^n\cdot\mathbf{F}_i^n - \mathbf{F}_i^o\cdot\mathbf{F}_i^o)\Big] \end{aligned} \tag{4.15}$$

The change in energy $(U_n - U_o)$ is familiar from the usual un-biased Monte Carlo algorithm and the remainder, which derives from enforcing detailed balance, serves to correct for the biasing of the moves in the direction of the acting force that results from applying equation 4.14

In brief, the Smart BD algorithm reads as follows:

1. Select a non-overlapping configuration.
2. Choose a random permutation of particle indices.
3. Sample a new position of particle 1 according to the Ermak scheme

4. Accept the move with probability $min(1, P_{o\to n})$. If the move is rejected the old state is counted again.

5. Repeat steps 3 and 4 until all particles had one chance to move.

6. Time is advanced by τ after each particle had a trial move.

where we have used Fisher-Yates shuffling [40] to generate the random permutations of particle indices in step 2 above.

The Smart BD algorithm fulfills detailed balance under all conditions. Correct equilibrium averages are obtained after equilibration even when a large τ is used and, hence, Smart BD allows for larger time steps than standard BD does. If the generated trajectories are used to calculate dynamic properties, like the mean-square displacement, the Smart BD algorithm becomes exact in the limit $\tau \to 0$ only, i.e. where all moves are accepted. In that case, the Smart-BD and the Ermak standard BD schemes are the same. The Smart BD algorithm can be extended to include hydrodynamic interactions [41] , i.e. when the particle mobility βD_0 depends on the configuration.

,

Chapter 5

Theories

As a potential of mean force and in many cases an effective pair potential can be obtained for the colloidal particles, statistical mechanics combined with theories developed for simple liquids can be used to describe the equilibrium behavior of a colloidal system. Because of this many existing theories can be directly applied to colloidal systems. However, in many cases they need to be modified to include, e.g. polydispersity, and for dynamic properties it is only appropriate in some circumstances to adopt directly a theory for simple liquids.

5.1 Correlation functions

The radial distribution function is an important property used to characterize the microstructure of a fluid. It expresses the probability to find a particle at a certain distance from another particle. The radial distribution function is directly measurable by microscopy experiments and indirectly by scattering experiments on colloidal dispersions. It also plays a central role in theories of liquid state. Numerical results for $g(r)$ can be compared with theoretical predictions and thus serve as a criterion to test a particular theory. Once $g(r)$ is known, and provided that the particles interact through a pair-wise additive interaction, all thermodynamic properties are accessible since they can be written as integrals over $g(r)$.

The total correlation function, $h(r_{12})$, defined as $h(r_{12}) = g(r_{12}) - 1$ was by Ornstein and Zernike divided into two parts, one direct and one indirect part [42]

$$h(r_{12}) = c(r_{12}) + \rho \int c(r_{13})h(r_{23})d\mathbf{r}_3 \tag{5.1}$$

The above Ornstein-Zernike (OZ) equation defines the direct correlation func-

tion $c(r)$, expressing the direct correlation between particle 1 and 2. The latter part corresponds to the indirect part of the total correlation function. The generalization of the OZ equation for mixtures is:

$$h_{ij}(r_{12}) = c_{ij}(r_{12}) + \rho \sum_l x_l \int h_{il}(r_{13}) c_{lj}(r_{23}) d\mathbf{r}_3 \tag{5.2}$$

where the sum runs over all components of the mixture and x_i is the mole fraction of component i. The integral equation theories are generally based on a number of exact relationships between different distribution functions. These relationships are turned into closed, solvable systems of equations by some approximate closure relation. A closure relation, known to give accurate results for systems with short range interactions, is the so-called Percus-Yevick (PY) approximation [42]:

$$g(r) \approx e^{-\beta u(r)} \left[1 + h(r) - c(r)\right] \tag{5.3}$$

$$c_{ij}(r) = (1 - e^{\beta u_{ij}(r)}))g_{ij} \tag{5.4}$$

The PY theory can be solved analytically for hard spheres [43, 44] and so-called adhesive hard spheres [45] but solutions are normally done numerically in an iterative manner.

The PY approximation is known to give accurate results for systems with short-range interactions. This is found to be the case for short-range attractions of the effective one-component description of the AO model but is not true for the binary AO system. Since the polymer-polymer direct correlation function vanishes in the PY approximation for the binary AO model, we are left with the following equations,

$$\begin{aligned} h_{cc}(r_{12}) &= c_{cc}(r_{12}) + \rho_c \int c_{cc}(r_{23}) h_{cc}(r_{13}) d\mathbf{r}_3 + \\ &\quad \rho_p \int c_{cp}(r_{23}) h_{cp}(r_{13}) d\mathbf{r}_3 \end{aligned} \tag{5.5}$$

$$h_{cp}(r_{12}) = c_{cp}(r_{12}) + \rho_c \int c_{cp}(r_{23}) h_{cc}(r_{13}) d\mathbf{r}_3 \tag{5.6}$$

$$h_{pp}(r_{12}) = \rho_c \int c_{cp}(r_{23}) h_{cp}(r_{13}) d\mathbf{r}_3 \tag{5.7}$$

involving the total and direct correlation functions, $h_{ij}(r)$ and $c_{ij}(r)$. As a further approximation one can replace equation 5.5 by the effective one-component equation: $h_{cc}^{\text{eff}}(r_{12}) = c_{cc}^{\text{eff}}(r_{12}) + \rho_c \int c_{cc}^{\text{eff}}(r_{23}) h_{cc}^{\text{eff}}(r_{13}) d\mathbf{r}_3$, where the colloids interact via the AO potential. This equation is solved subject to the one-component Percus-Yevick closure, which leads to a revised PY theory.

Since the AO potential contains the polymer fugacity z_p rather than ρ_p, a connection between them is needed. This is given by equation 3.6, which is exact for $\xi \lesssim 0.1547$.

As shown in Paper I, a second approximate theory can be derived by neglecting higher order correlation functions. This gives expressions for g_{cp} and g_{pp} as integrals over g_{cc}. Once we have g_{cc} from solving the one-component PY theory with the AO potential, these can be determined. In Paper I this approximation is shown to be slightly worse than the revised PY theory.

5.2 Semi-grand-canonical ensemble and free-volume fraction

Considering a colloid-polymer mixture in which the polymers are in equilibrium with a reservoir, the natural statistical mechanic ensemble to choose is the semi-grand-canonical ensemble in which the polymer fugacity, $z_p = \lambda_p^{-3} e^{\beta\mu_p}$, is fixed along with the number of colloids N_c , the volume V, and the temperature T. μ_p and λ_p denote the chemical potential and the thermal de Broglie wavelength respectively of the polymer coils. The two-component partition function is in the semi-grand-canonical ensemble defined as:

$$\psi = \sum_{N_p=0}^{\infty} \frac{z_p^{N_p}}{N_p!} \frac{1}{N_c! \lambda_c^{3N_c}} \int d\mathbf{r}^{N_p} \int d\mathbf{R}^{N_c} e^{-\beta U(\mathbf{R}^{N_c}, \mathbf{r}^{N_p})} \tag{5.8}$$

where the subscripts c and p denote colloids and polymers, respectively, U is the potential energy, and $\mathbf{R}$ and $\mathbf{r}$ denote the colloid and polymer coordinates, respectively. Differentiating with respect to z_p one readily obtains

$$\left(\frac{\partial \ln \psi}{\partial z_p} \right)_{V,T,N_c} = \frac{\langle N_p \rangle}{z_p} \tag{5.9}$$

where $\langle \cdot \rangle$ is a semi-grand-canonical ensemble average. If the polymers are taken as ideal, i.e. $z_p = \rho_p^r$, the above yields a relation for the so-called free-volume fraction $\alpha = \rho_p / \rho_p^r$.

In addition, for the AO system in which the polymers do not interact with themselves, $u_{pp} = 0$, it is useful to define an effective colloid potential

as

$$
\begin{aligned}
e^{-\beta\Omega(\mathbf{R}^{N_c})} &= \sum_{N_p=0}^{\infty} \frac{z_p^{N_p}}{N_p!} \int e^{-\beta \sum_{i=1}^{N_c} \sum_{j=1}^{N_p} u_{cp}(\mathbf{R}_i - \mathbf{r}_j)} d\mathbf{r}^{N_p} \\
&= \sum_{N_p=0}^{\infty} \frac{1}{N_p!} \left(z_p \int e^{-\beta \sum_{i=1}^{N_c} u_{cp}(\mathbf{R}_i - \mathbf{r}_j)} d\mathbf{r}_j \right)^{N_p} \\
&= e^{z_p \int e^{-\beta \sum_{i=1}^{N_c} u_{cp}(\mathbf{R}_i - \mathbf{r}_j)} d\mathbf{r}_j} \qquad (5.10)
\end{aligned}
$$

where $e^x = \sum_{n=0}^{\infty} \frac{x^n}{n!}$ was used in the last step. As shown first by Gast et al. [12] and later by Brader et al. [24] for the AO system, for size ratios $\sigma_p/\sigma_c \leq 2/\sqrt{3} - 1 \approx 0.1547$ the effective potential is exactly pair-wise additive and given by

$$
-\beta\Omega(\mathbf{R}^{N_c}) = z_p V - \frac{\pi}{6} z_p N_c (\sigma_c + \sigma_p)^3 - \beta \sum_{i>j}^{N_c} u_{AO}(R_{ij}) \qquad (5.11)
$$

where the effective AO potential is given by equation 3.5. Inserting equation 5.10 in the partition function in equation 5.8 and using equation 5.9 leads to an insertion formula [46] for the free-volume fraction

$$
\alpha = \left\langle e^{-\beta \sum_{i=1}^{N_c} u_{cp}(|\mathbf{R}_i - \mathbf{r}|)} \right\rangle \qquad (5.12)
$$

where the average is the configurational average in the one-component colloidal system with particles interacting via the effective AO potential. By similar steps, insertion formulas can be derived for the pair correlation functions involving the polymers. The polymer-polymer radial distribution function is given by

$$
g_{pp}(|\mathbf{r}_1 - \mathbf{r}_2|) = \alpha^{-2} \left\langle e^{-\beta \sum_{i=1}^{N_c} u_{cp}(|\mathbf{R}_i - \mathbf{r}_1|)} e^{-\beta \sum_{i=1}^{N_c} u_{cp}(|\mathbf{R}_i - \mathbf{r}_2|)} \right\rangle \qquad (5.13)
$$

and the colloid-polymer radial distribution function is found from

$$
g_{cp}(|\mathbf{r}|) = \alpha^{-1} \left\langle e^{-\beta \sum_{i=1}^{N_c} u_{cp}(|\mathbf{R}_i - \mathbf{r}_1|)} V \delta(\mathbf{R}_1 - (\mathbf{r} + \mathbf{r}_1)) \right\rangle \qquad (5.14)
$$

where the delta function indicates that insertions of a polymer sphere are made relative to a colloidal particle in the mixture. In all cases the insertions are made in a system governed by the colloid-colloid potential u_{cc} plus the effective potential in equation 5.11. In other words, the pair correlations can be determined by inserting one or two polymer spheres in the colloidal system by a MC simulation scheme for any value of z_p even though the polymers are not present explicitly in the system.

5.3 Free-volume theory of colloid mixtures

Generalizing the semi-grand-canonical ensemble to a $(M+1)$-component system, where again, the polymers are in osmotic equilibrium with a reservoir gives the following partition function

$$\begin{aligned}\psi(z_p, N_1, \ldots, N_M, V, T) &= \sum_{N_p=0}^{\infty} \frac{z_p^{N_p}}{N_p!} \frac{1}{N_1!\lambda_1^{3N_1} \cdots N_M!\lambda_M^{3N_M}} \times \\ &\int e^{-\beta U(\mathbf{r}^{N_p}, \mathbf{R}^{N_c})} d\mathbf{r}^{N_p} d\mathbf{R}^{N_c} \end{aligned} \tag{5.15}$$

where $N_c = N_1 + \ldots + N_M$, and as before lower-case coordinates are used to distinguish the N_p polymers from the remaining enclosed particles.

Interpreting $-k_BT \ln \psi$ as a Helmholtz energy $A(z_p, N_1, \ldots, N_M, V, T)$, we can integrate equation 5.9

$$\begin{aligned}A(z_p, N_1, \ldots, N_M, V, T) &= A(0, N_1, \ldots, N_M, V, T) + \\ &\int_0^{z_p} \alpha(z_p', N_1, \ldots, N_M, V, T) dz_p' \end{aligned} \tag{5.16}$$

which is the starting point for the so-called free-volume theory. If we follow Lekkerkerker et al. [13] in their work on monodisperse systems and assume that the free-volume fraction in equation 5.16 can be replaced by $\alpha(z_p = 0, N_1, \ldots, N_M, V, T)$, we obtain

$$\begin{aligned}A(z_p, N_1, \ldots, N_M, V, T) &= A(0, N_1, \ldots, N_M, V, T) + \\ &z_p \alpha(0, N_1, \ldots, N_M, V, T) \end{aligned} \tag{5.17}$$

We note that $A(0, N_1, \ldots, N_M, V, T)$ and $\alpha(0, N_1, \ldots, N_M, V, T)$ are quantities for a hard-sphere mixture for which approximate expressions are available from the so-called BMCSL equation of state [47–49] and the scaled-particle theory [50]. When these are substituted in, an analytical expression for the free energy is obtained and one can find the chemical potentials from $\mu_\alpha = \frac{\partial A}{\partial N_\alpha}$ and the osmotic pressure from $\Pi = -\frac{\partial A}{\partial V}$. For a mixture of a few components it is possible to solve the set of coupled equations that one gets from equating chemical potentials and osmotic pressures between phases. This leads to predictions of the fluid phase behavior of the mixture, which can be used to understand qualitatively how a system phase separates into coexisting phases not only with different overall volume fractions but also with different compositions.

5.4 Mode coupling theory of glass transitions

The theory known as mode coupling theory (MCT) has been very successful at describing the dynamics of dense atomic and colloidal systems [51]. It also provides an idealized mechanism for the glass transition in such systems, namely as a transition to a nonergodic state where particle positions remain correlated in the limit of long times [52]. The interpretation is that this transition is caused by particles becoming trapped in cages made up by the nearest neighbors. In the following a brief presentation is given of the elegant derivation due to Zaccarelli et al. [53] of the MCT. It is based on classical Newtonian dynamics but the same result is also obtained for diffusive dynamics appropriate for colloids if hydrodynamic interactions are neglected [54].

Zaccarelli and co-workers consider the fluctuating number density $\rho(\mathbf{r},t) = \sum_{j=1}^{N}\delta(\mathbf{r}-\mathbf{r}_j(t))$ and its Fourier transform $\rho(\mathbf{k},t) = \sum_{j=1}^{N} e^{i\mathbf{k}\cdot\mathbf{r}_j(t)}$. An equation of motion for the number density is obtained by examining the second time derivative

$$\ddot{\rho}(\mathbf{k},t) = \sum_{j=1}^{N} i\mathbf{k}\cdot\ddot{\mathbf{r}}_j(t)e^{i\mathbf{k}\cdot\mathbf{r}_j(t)} + \sum_{j=1}^{N}(i\mathbf{k}\cdot\dot{\mathbf{r}}_j(t))^2 e^{i\mathbf{k}\cdot\mathbf{r}_j(t)} \tag{5.18}$$

and substituting in Newton's second law for a pair-wise additive interaction potential

$$\begin{aligned} m\ddot{\mathbf{r}}_j(t) &= -\sum_{l=1,l\neq j}^{N}\frac{\partial}{\partial\mathbf{r}_j}u(|\mathbf{r}_j-\mathbf{r}_l|) \\ &= (2\pi)^{-3}\int(i\mathbf{k}')e^{-i\mathbf{k}'\cdot\mathbf{r}_j}u(\mathbf{k}')\rho(\mathbf{k}',t)d\mathbf{k}' \end{aligned} \tag{5.19}$$

where it was assumed that the pair potential can be Fourier transformed. Using equation 5.19 in equation 5.18 results in an equation describing the dynamic behavior of the number density

$$\begin{aligned} m\ddot{\rho}(\mathbf{k},t) &= \mathcal{F}(\mathbf{k},t) \\ &= -(2\pi)^{-3}\int(\mathbf{k}\cdot\mathbf{k}')u(\mathbf{k}')\rho(\mathbf{k}',t)\rho(\mathbf{k}-\mathbf{k}',t)d\mathbf{k}' - \\ &\quad m\sum_{j=1}^{N}(\mathbf{k}\cdot\dot{\mathbf{r}}_j(t))^2 e^{i\mathbf{k}\cdot\mathbf{r}_j(t)} \end{aligned} \tag{5.20}$$

where $\mathcal{F}(\mathbf{k},t)$, can be thought of as a force simply from the analogy with Newton's second law. The next step is to divide this force in a part that

is correlated with the number density and another part that is not. It is possible to show that

$$\left\langle \rho(-\mathbf{k},t)\left[\mathcal{F}(\mathbf{k},t)-\frac{k_BTk^2\rho(\mathbf{k},t)}{S(k)}\right]\right\rangle = 0 \tag{5.21}$$

where the static structure factor is defined as $S(k)=N^{-1}\left\langle\rho(-\mathbf{k},t)\rho(\mathbf{k},t)\right\rangle$ and where $\langle\cdot\rangle$ is an equilibrium average in the canonical ensemble. Another, so-called residual force is then defined by writing

$$m\ddot{\rho}(\mathbf{k},t)+\frac{k_BTk^2}{S(k)}\rho(\mathbf{k},t) = \mathcal{F}^{\text{resid}}(\mathbf{k},t) \tag{5.22}$$

which is totally uncorrelated with the number density. The reason for this division is that the number density is a conserved variable because the number of particles and the volume are constant. The number density in a part of the system can then only change value by particles moving a significant distance and it is therefore expected to change slowly in time. One can then hope that $\mathcal{F}^{\text{resid}}(\mathbf{k},t)$, because it is uncorrelated with the number density, changes faster and is of less importance for the dynamics at long times.

The residual force is written as a sum of a dissipative term with a so-called memory function and a noise term, according to

$$\mathcal{F}^{\text{resid}}(\mathbf{k},t) = -\int_0^t \gamma(\mathbf{k},t-t')\frac{\partial\rho(\mathbf{k},t')}{\partial t'}dt'+f^{\text{noise}}(\mathbf{k},t) \tag{5.23}$$

where $\gamma(\mathbf{k},t)$ is the memory function, which describes how the current state of the system depends on its past. The memory and noise are related through a fluctuation-dissipation theorem (FDT),

$$\begin{aligned}\langle f^{\text{noise}}(\mathbf{k},t)\rangle &= 0\\ \langle f^{\text{noise}}(-\mathbf{k},t)f^{\text{noise}}(\mathbf{k},t')\rangle &= Nk_BTk^2\gamma(\mathbf{k},t-t')\end{aligned} \tag{5.24}$$

which guarantees that the system evolves to the correct Boltzmann equilibrium distribution. An exact expression can be derived for the memory function [53] by substituting equation 5.23 and the expression for $\mathcal{F}^{\text{resid}}(\mathbf{k},t)$ (from equations 5.20 and 5.22) into equation 5.24. In it appears averages of multiple number densities, i.e. products of number densities. If the number density itself evolves slowly in time then it is possible that such averages also change slowly in time. The mode coupling theory aims to take account of this additional slowness. It is obtained from the exact memory function by assuming the noise and the number density are fluctuating Gaussian variables.

This means Wick's theorem applies and multiple averages of number densities can be reduced to averages of products of only two number densities [55]. With this assumption the memory function becomes [53]

$$\begin{aligned}\gamma(\mathbf{k},t) &\approx \rho^2 k_B T k^2 S(k,t)\left(c(k)+\beta u(k)\right)^2 - \\ &\quad \rho\left(\beta u(k)+c(k)\right)\int_0^t \gamma(\mathbf{k},t-t')\frac{\partial S(k,t')}{\partial t'}dt' + \\ &\quad \frac{\rho}{2(2\pi)^3 k_B T k^2}\int\left[(\mathbf{k}\cdot\mathbf{k}')u(k')(\mathbf{k}\cdot(\mathbf{k}-\mathbf{k}'))u(|\mathbf{k}-\mathbf{k}'|)\right]^2 \times \\ &\quad S(k',t)S(|\mathbf{k}-\mathbf{k}'|,t)d\mathbf{k}'\end{aligned}$$

where $S(k,t) = N^{-1}\left\langle\rho(-\mathbf{k},0)\rho(\mathbf{k},t)\right\rangle$ is the dynamic structure factor. However, if the number density is a fluctuating Gaussian quantity then the so-called random phase approximation (RPA) applies, which means that the direct correlation function is just $c(k) = -\beta u(k)$. Thus the following simpler, mode coupling expression is obtained

$$\begin{aligned}\gamma(\mathbf{k},t) &\approx \frac{\rho k_B T}{2(2\pi)^3 k^2}\int\left[(\mathbf{k}\cdot\mathbf{k}')c(k')+(\mathbf{k}\cdot(\mathbf{k}-\mathbf{k}'))c(|\mathbf{k}-\mathbf{k}'|)\right]^2 \times \\ &\quad S(k',t)S(|\mathbf{k}-\mathbf{k}'|,t)d\mathbf{k}'\end{aligned} \tag{5.25}$$

where the direct correlation function replaces the pair potential. However, in actual applications of mode coupling theory the RPA closure is typically not used, thus violating the consistency of the approximation.

In experiments one measures the dynamic structure factor, which is governed by the following equation of motion (obtained from equation 5.22),

$$m\ddot{S}(k,t)+\frac{k_B T k^2}{S(k)}S(k,t) = -\int_0^t \gamma(\mathbf{k},t-t')\frac{\partial S(k,t')}{\partial t'}dt' \tag{5.26}$$

When taken together with the mode coupling approximation in equation 5.25 it is seen to be fully predictive for $S(k,t)$ if the direct correlation function is specified. It is also a non-linear equation with respect to $S(k,t)$. If one defines $f(k,t) = S(k,t)/S(k)$ and $f(k) = f(k,t\to\infty)$ and takes the limit $t\to\infty$ in equation 5.26, the following equation is obtained

$$\begin{aligned}\frac{f(k)}{1-f(k)} &= \frac{\rho}{2(2\pi)^3 k^4}\int S(k)S(k')S(|\mathbf{k}-\mathbf{k}'|)\times \\ &\quad \left[(\mathbf{k}\cdot\mathbf{k}')c(k')+(\mathbf{k}\cdot(\mathbf{k}-\mathbf{k}'))c(|\mathbf{k}-\mathbf{k}'|)\right]^2 \times \\ &\quad f(k')f(|\mathbf{k}-\mathbf{k}'|)d\mathbf{k}'\end{aligned} \tag{5.27}$$

which was first derived by Bengtzelius et al. [52]. It can be solved for $f(k)$ by iteration. The result $f(k) = 0$ is always a solution to equation 5.27,

implying that the dynamic structure factor decays to zero as expected for liquids. However, for strong interactions $f(k) \neq 0$ is also a solution, and it has been shown to be the correct solution for $S(k, t \to \infty)/S(k)$ [56]. This means that $S(k, t)$ does not decay to zero and that particles are correlated even in the limit $t \to \infty$, which describes a glass transition, though idealized in the sense that real systems usually exhibit some slow relaxation towards equilibrium.

,

Chapter 6

Results

6.1 Summary of Paper I

Prediction of structures and gel transitions in systems of colloids with moderate-range attractions

The purpose of Paper I is to provide a careful assessment of the accuracy of the effective one-component description of the depletion interaction within the Asakura-Oosawa (AO) theory. Furthermore, some approximate theories for the radial distribution functions are developed and tested against MC simulation results. In addition, these liquid structure theories are used as input to MCT to obtain predictions for the occurance of so-called attractive glass states.

From previous work it is known that for polymer-colloid size ratios above $\xi \approx 0.1547$ the mapping between the binary AO model and the effective one-component description of the same model is not exact since effects of many-body correlations start to contribute [12, 24]. As a consequence, the full interaction is no longer given by a pair-wise addition of the AO pair potential. To examine whether, in spite of this, the effective one-component model gives a fair description of the binary AO model also for the size ratio $\xi = 0.25$, we compare liquid structures as obtained from the effective one-component description with those obtained from the binary version of the model. As seen in figure 6.1, the two determinations of the colloid-colloid radial distribution functions g_{cc} resulting from the different descriptions agree closely, both concerning the overall shape and also in the contact value of the radial distribution functions. Note that the one-component model is even able to capture the splitting of the second peak of g_{cc}. This feature is usually associated with metastable or precursor states close to crystallization [57]. To

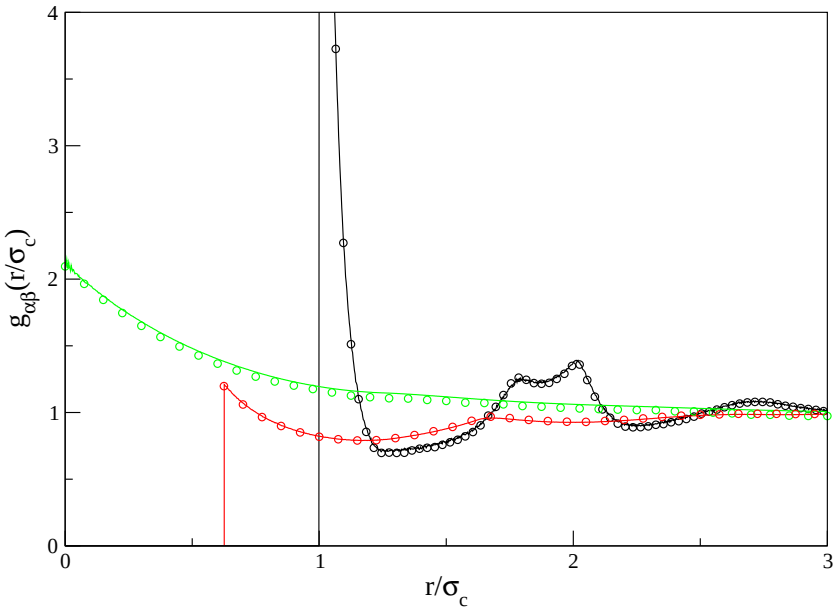

Figure 6.1: Radial distribution functions g_{cc}, g_{cp}, and g_{pp} as a function of the separation distance normalized by the colloid diameter for $\xi = 0.25, \phi_c = 0.30, \phi_p = 0.20$, and $\phi_p^{(R)} = 0.42$. The lines correspond to MC simulations of the binary AO model and the symbols to MC simulations of the effective one-component system interacting via the AO potential combined with the particle insertion method.

compare the results of the two models it is necessary to apply some iterations, because $\phi_p^{(R)}$ instead of ϕ_p enters in the one-component model. Therefore, given ϕ_p from a simulation of the binary system one has to estimate $\phi_p^{(R)}$ to be used for the one-component simulation from which ϕ_p is determined by random insertion of a polymer sphere (cf. equation 5.12). In figure 6.1, also the colloid-polymer radial distribution function g_{cp} and polymer-polymer radial distribution function g_{pp} as obtained by the two descriptions are compared. Polymers are not explicitly present in the effective one-component description, but, as described in section 5.2. and as derived in Paper I, it is nevertheless possible to extract the remaining radial distribution functions. Since the presence of polymer is reflected in the configurations of colloidal particles, which are seen to be essentially the same from g_{cc} in figure 6.1, the configurations can be sampled by insertions of polymer particles. Inserting one or two polymer spheres during the course of a MC simulation within the effective one-component AO model lets one determine g_{cp} and g_{pp}. Here, these distribution functions are used to determine whether the mapping remains accurate for the complete pair-level structure for this size ratio. Again

the results from the two different descriptions agree closely, and it follows that for $\xi = 0.25$ the pair-wise additivity of the AO potential is an excellent approximation, i.e. the effective one-component model remains an accurate description of the AO model. Note that the insertion procedure for g_{cp} and g_{pp} is only exact below $\xi \approx 0.1547$ but that it then holds for any polymer concentration.

Percus-Yevick (PY) integral equation theory is known to provide good results for short-ranged attractions [42]. This holds also in the case of the effective one-component AO model. In general, PY theory compares favorably for low to moderate polymer concentrations. For high polymer concentrations the theory tends to overestimate somewhat the contact value of the radial distribution function. Overall, however, PY theory provides near-quantitative predictions for the colloidal microstructure in the single-phase fluid regime. As shown in Paper I, this holds also in terms of the colloid-colloid structure factor, $S_{cc}(k)$. Deviations between PY theory and simulation results for $S_{cc}(k)$ appear, however, when polymer concentrations become high.

While PY theory captures the liquid structure well for the one-component AO system, the two-component version of the theory does so only when the polymer concentration is kept low. Exploiting that accurate results are obtained for the one-component PY theory, we suggest in Paper I two approximate theories to predict the remaining radial distribution functions. The so-called revised PY theory as described in section 5.1 is in good agreement with the simulation result for g_{cp} but underpredicts somewhat the result for g_{pp}, where it fails to produce the expected result, $g_{pp}(0) = 1/\alpha$ [58]. A so-called low-order approximation slightly overpredicts the simulation result for the first correlation peak and is slightly low just prior to the second peak in g_{cp}. It tends to overpredict the small-r structure of g_{pp}. The predictions improve on the whole, however, with decreasing size ratio, but the revised PY integral equation theory appears to give better structural predictions.

The ability of the MCT to model the low-density gel transitions for moderate-range attractive systems is tested. This is done within the AO model and the results are compared with experimental data. Results are reported for larger polymer-colloid size ratios that what has been reported on before but still sufficiently small that gel states have been recorded experimentally. As already discussed, PY integral equation theory produces accurate liquid structures for size ratios of ≈ 0.25 and it is used to provide the static input needed for MCT. Analyzing the glass transitions as predicted by MCT for the size ratios $\xi = 0.20, 0.25$, and 0.30, it is found that for $\phi_p^{(R)} = 0$ the glass transition starts at the hard-sphere glass transition value, $\phi_c = 0.5159$ [52], using PY as input. For small values of $\phi_p^{(R)}$ the

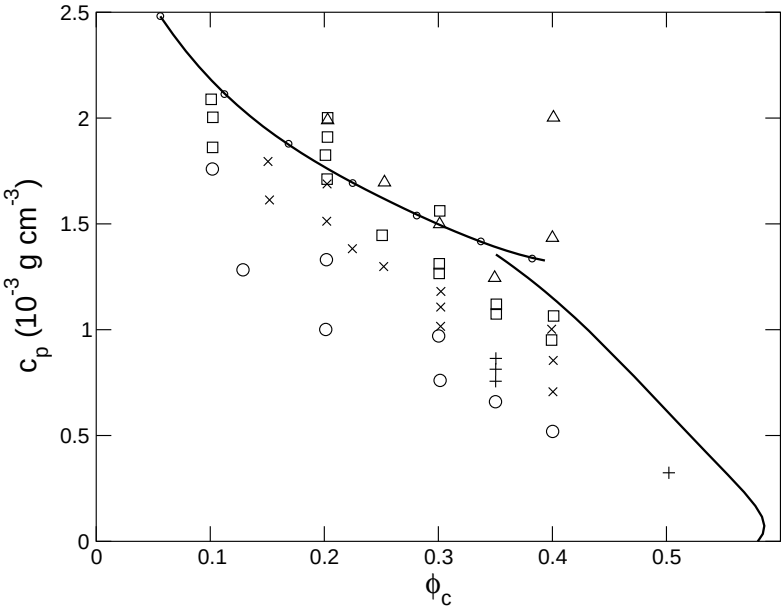

Figure 6.2: Comparison of MCT prediction for the glass transition against experiments on model colloid-polymer mixtures for $\xi \approx 0.24$, reproduced from [22], in terms of polymer mass concentration and colloid volume fraction. The symbols denote experimental data: fluid(circle), liquid + crystal (plus), gas + crystal (square), glass + liquid + crystal (cross) , and no visible crystallization (triangle). The line is the MCT prediction along with the PY spinodal (marked by small circles) for $\xi = 0.25$. Note that the colloid volume fraction in the theoretical predictions has been shifted to agree with the experimental glass transition value for hard spheres, $\phi_c \approx 0.58$ [10, 59, 60], viz. $\phi_c = \phi_c^{theory} 0.58/0.516$.

transition tends to larger colloid volume fractions, but when increasing the polymer volume fraction further the glass transition starts to migrate toward lower ϕ_c. It follows that there is a small region of reentrant glass melting, meaning one goes from glass to fluid to glass again at the same particle volume fraction by adding polymers. For the three size ratios studied here, increasing the polymer concentration sufficiently leads to the MCT transitions meeting the PY spinodal on the dense fluid side in all cases, but as the attraction range is reduced the transition occurs closer to the critical point.

A detailed experimental phase diagram, identifying locations of not only equilibrium phase coexistence but also non-ergodic gel states, is available from the work of Ilett and co-workers for $\xi \approx 0.24$ [22]. This phase diagram is reproduced in figure 6.2 in terms of added polymer mass concentration and colloid volume fraction. Included in the figure is the MCT prediction for the glass transition along with the PY prediction for the spinodal for $\xi = 0.25$.

There is reasonable agreement between results from theory and considering there are no adjustable parameters except for ξ. For the $\xi = 0.25$ size ratio the predicted glass transition line has a slope that agrees approximately with the cessation of crystal formation in the experiments, which we interpret as non-ergodic gels.

6.2 Summary of Paper II

Equilibration of fluid-phase coexistence in polydisperse particle systems with short- and moderate-range depletion attractions

In Paper II a study of the fluid-fluid coexistence of systems interacting via the AO potential is undertaken. The aim is to examine to what extent Gibbs ensemble Monte Carlo (GEMC) simulations can be used to obtain phase equilibrium data for systems with short ranges of attraction.

For short-range attractive systems the fluid-fluid binodal is metastable with respect to crystallization [12, 13, 61]. In spite of its metastability there is considerable interest in determining the location of this transition. Since crystallization is usually a slow process the metastable fluid behavior can sometimes be observed for long times [62]. Also, the fluid-fluid transition, even though it is metastable, can affect how fast crystallization occurs and also the quality of the crystals [63]. Also, polydisperse samples may not crystallize, in which case the fluid-fluid transition becomes an equilibrium transition also for short-range attractive systems. In this study size-polydispersity was incorporated into the AO model to avoid effects of crystallization, i.e. the interactions were described by equation 3.7.

The GEMC method is generally well suited to simulate fluid-fluid coexistence. However, it is not always straightforward to determine the location of the fluid-fluid transition for short-range attractive systems. In this case particles exhibit an increased tendency to stick to one another in long-lived aggregates, and sampling in phase space becomes difficult, as does the determination of points on the coexistence curve [64]. This is indeed what we find in applying the GEMC method directly for the short-range polydisperse AO model, where the interaction range corresponds to a dimensionless polymer size $\xi = 0.10$. This is illustrated in figure 6.3 where the resulting phase diagram is shown in terms of polymer and colloid volume fractions, with the circles having been generated from the same initial crystalline lattice. Filled and open circles correspond to results obtained with two different random number generator seeds. The triangles in the same figure corresponds

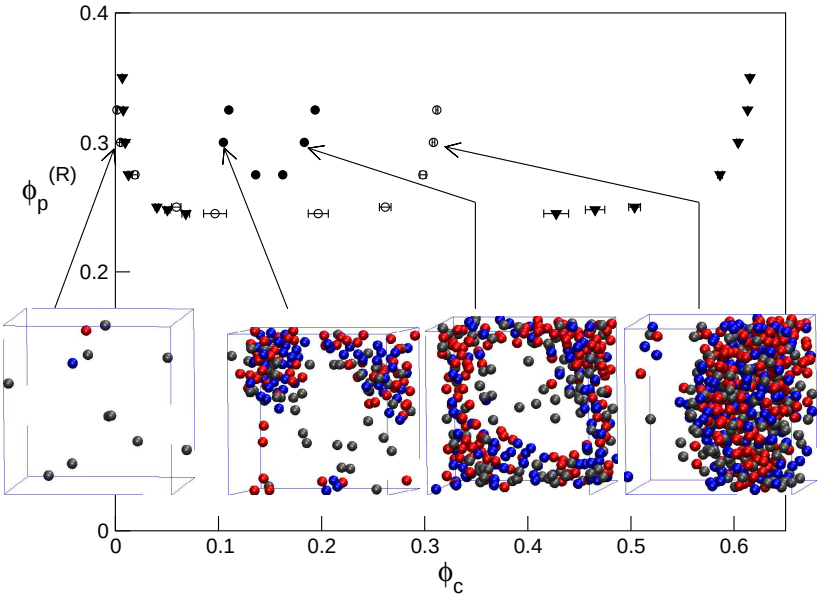

Figure 6.3: Resulting "phase diagram" for the polymer-colloid size ratio $\xi = 0.10$ in terms of polymer reference and colloid volume fractions, with the circles having been generated from the same initial crystalline lattice. Filled and open circles correspond to results obtained with two different sequences of random numbers. Nearly equilibrated points of fluid-fluid coexistence are shown as triangles. The insets show the end configurations of the equilibration period corresponding to $\phi_p^{(R)} = 0.30$ and at colloid volume fractions as indicated by the arrows. Colloid polydispersity is mimicked by three discrete particle sizes: small (grey), middle (red), and large (blue).

to the (nearly) equilibrated fluid-fluid coexistence curve. One sees that the simulations get stuck on the way towards equilibrium. Inset into the figure are snapshots of configurations at compositions as indicated by the arrows. These configurations are characterized by large-scale inhomogeneities in the form of clusters and voids in at least the denser of the two simulation boxes. Both the clusters and voids reach the size of the simulation box, leading to only small volume changes being accepted in the GEMC simulation.

For longer-range attractions, greater than about 50% of the particle diameter, the convergence towards equilibrium proceeds smoothly. On taking an equilibrated configuration for a longer-range depletion attraction as a starting configuration for a GEMC simulation at a somewhat shorter-range attraction, the phase coexistence curve is moved in the phase diagram as seen

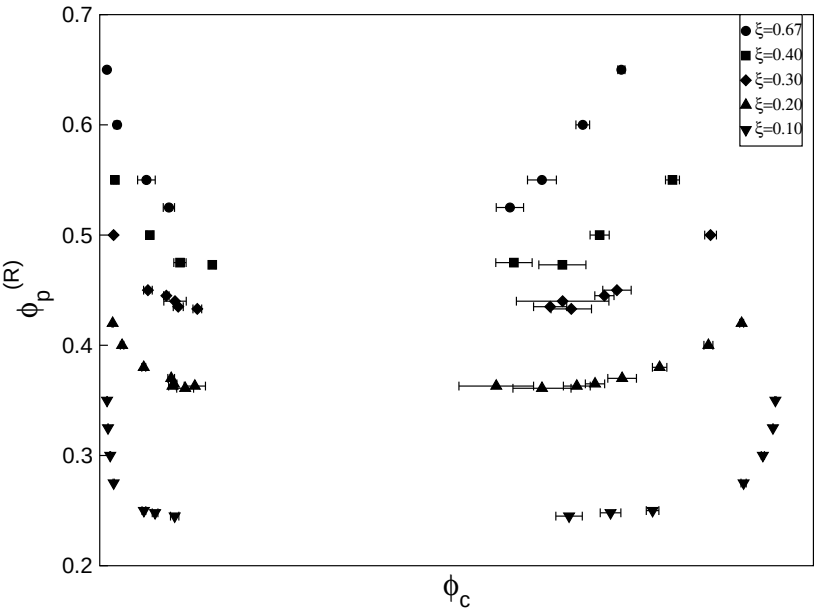

Figure 6.4: Fluid-fluid coexistence data in terms of polymer reference and colloid volume fractions for different dimensionless polymer sizes ξ, as labeled.

in figure 6.4. The dense phase is further densified whereas the dilute-fluid phase becomes more dilute. The stepwise movement of the fluid-fluid coexistence envelope persists even on reaching polymer-colloid size ratios that would get pinned during direct equilibration. Furthermore, we find that the chemical potentials of the species [33, 65] reach equal values in the two simulation boxes within error bars. However, in contrast to the simulations for the medium- and longer-range attractions, it becomes difficult to ascertain whether equilibrium has been reached for $\xi = 0.1$. One test is given by recovery of the phase boundary on perturbing the systems. Taking the configuration for $\xi = 0.1$ at the highest $\phi_p^{(R)}$ in figure 6.4 as input, several of the remaining coexistence pairs of volume fractions in figure 6.4 for $\xi = 0.1$ could be reproduced within error bars. This suggests that in terms of the overall concentration the system reaches equilibrium also for this shorter depletion range.

The chemical potentials of the small- and medium-size particles in the dilute fluid vary smoothly and rapidly settle at steady values while the chemical potential of the large-size particles in the dilute phase shows some smaller jumps before it eventually converges. However, the chemical potentials of the species in the dense fluid phase are slow to converge to steady values and exhibit occasional jumps during the accumulation of data for the ensemble averages. The jumps are caused by individual particle insertions that some-

times result in very low energies and therefore very large contributions to the ensemble average in the expression for the chemical potential (cf. equation 4.10). To obtain reasonable averages in these cases it is necessary to sample many such rare, low-energy insertions, which requires very long simulation runs. Equilibrium is eventually reached for the small- and medium-size components for the lower $\phi_p^{(R)}$ but some of the larger particles never enter the dilute phase in spite of thousands of attempts. In other words, for most of the points on the $\xi = 0.10$ curve in figure 6.4 compositional equilibrium is not reached, presumably due to some of large particles clusters that remain intact throughout the simulations.

6.3 Summary of Paper III

Brownian dynamics of colloidal liquids characterized by short-range depletion interactions

In this paper we examine how the structures in the concentrated phases generated by the GEMC method in Paper II behave dynamically. In Paper II for the smallest polymer-colloid size ratios it was found that some particles, particularly the large ones, did not transfer between phases and that full phase equilibrium was not reached because of this. This effect was attributed to the fact that large particles attract each other more strongly and that some structures of these are formed that cannot be broken up easily by Monte Carlo moves. It is thus of interest to see whether these structures can be identified in simulations of the dynamics.

Colloidal particles undergo Brownian motion and Ermak's Brownian dynamics (BD) algorithm based on the position-Langevin equation captures this process if hydrodynamic interactions are neglected [34]. The Ermak algorithm cannot be used with hard-sphere or other discontinuous interactions and it is therefore most common to use a steep but smooth repulsion in the interaction potential. This mean that small displacements of particles can result in very large forces and because the Ermak algorithm is only correct to leading-order in time such interactions require very small time steps. As described in section 4.2 the so-called Smart BD method [35–39] uses instead Monte Carlo moves to accept or reject trial displacements generated from the Ermak algorithm and it is therefore well suited to dealing with hard-sphere interactions. However, the trajectories generated by Smart BD are known to depend on the time step used [38]. To take account of this dependence, a rescaling of time by the fraction of accepted moves has been suggested [36]. We verify in Paper III that applying this rescaling results in mean-square dis-

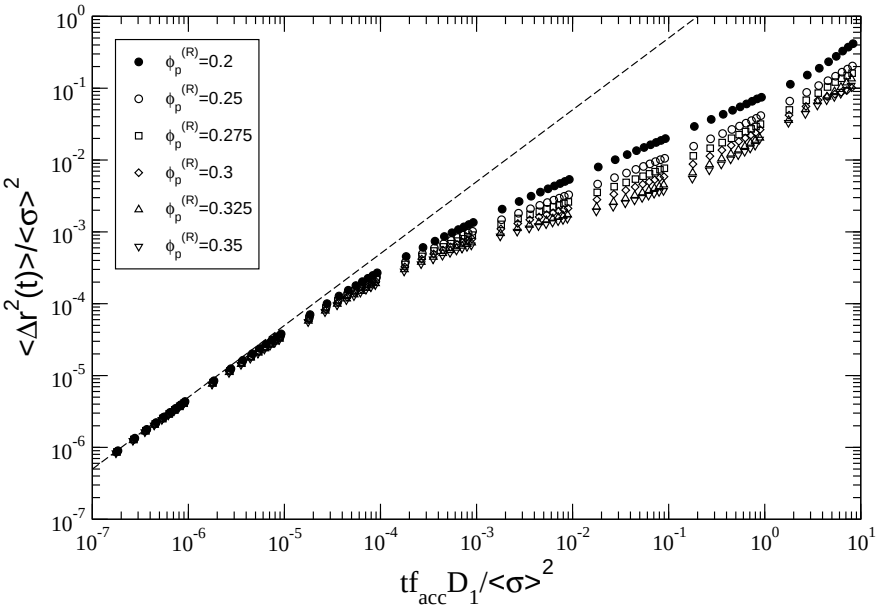

Figure 6.5: Mean-square displacement of particles at $\phi_c = 0.605$ as a function of time and polymer concentration as labeled. The dashed line shows the short-time behavior given by the average Stokes-Einstein diffusion coefficient $\langle D \rangle = 0.832 D_1$ in terms of the diffusion coefficient of the small spheres D_1.

placements that overlap for concentrated systems even though very different time steps are used, which means that Smart BD simulations can be run to times that are of interest in studies of structural slowing down in connection with glass formation.

The mean-square displacement characterizes the average movement of particles as a function of time. According to Einstein [66], a diffusion coefficient can be defined when the mean-square displacement becomes a linear function of time. Figure 6.5 shows the mean-square displacement as a function of time and polymer concentration for a highly concentrated system at a volume fraction of $\phi_c = 0.605$. At short times the mean-square displacement is linear with a slope given essentially by the Stokes-Einstein diffusion coefficient. At very long times it almost becomes a linear function again, but with a much smaller slope characterized by the long-time self-diffusion coefficient. As the polymer concentration is increased, which moves the system towards the fluid-fluid phase transition, the mean-square displacement is gradually slowed down. However, for all the systems studied the mean-square displacement is an increasing function of time and no arrest of the dynamics is found. In the GEMC simulations in Paper II, some percentage of particles, particularly the large ones, were localized throughout the simulations. In GEMC

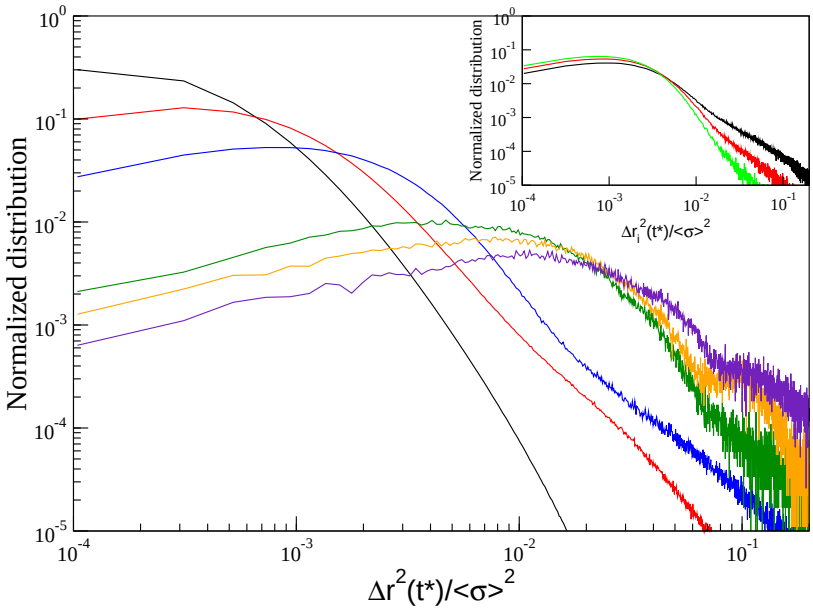

Figure 6.6: Distribution of squared displacements of particles for $\phi_c = 0.614$ and $\phi_p^{(R)} = 0.325$ at specific times t^*. The distributions decrease in height along the left-hand side as a function of time in the following order $t^* D_1/\langle\sigma\rangle^2 = 9.1 \cdot 10^{-4}$, $2.3 \cdot 10^{-2}$, 0.24, 2.3, 4.3, and 7.3 where D, is the diffusion coefficient of the smallest particles in the mixture. The inset shows the distribution for $t^* D_1/\langle\sigma\rangle^2 = 0.24$ with the three components resolved according to, from top to bottom along the left-hand side, large-, middle-, and small-size particles, showing that the small particles make up most of the "fast" tail of the distribution.

one attempts to exchange particles between the dense fluid and a dilute fluid. Such moves are often associated with large energy increases, and they are as a consequence most often rejected by the Monte Carlo algorithm. In the dense fluids, studied here in isolation, the surrounding particle structure provides a scaffold of low-energy particle-particle contacts on which any given particle can diffuse dynamically without experiencing too much of an energy change.

Figure 6.6 demonstrates that the dynamics of the displacements is not simple. It shows the probability distribution for particles having reached a certain squared displacement after a certain time. This distribution is shown for several different times, ranging from those where particles have not yet passed the range of attraction to those where they have reached as much as a particle radius. The distributions broaden as time progresses and eventually develop a tail at intermediate times when a fraction of the particles have passed the range of the attraction. For the longest times shown in figure 6.6 the distribution develops a shoulder near a squared displacement of $0.1\langle\sigma\rangle^2$.

This corresponds to distances significantly greater than the range of the depletion attraction and it is more likely to be connected to the cage of nearest neighbors, which particles need to penetrate and escape from for structural relaxation to occur. Presumably, for somewhat higher particle concentrations, this shoulder might develop into a separate peak corresponding to a population of fast particles as has been observed for glassy systems [67, 68].

6.4 Summary of Paper IV

Low-density nonergodicity transitions from the idealized mode coupling theory

Applying mode-coupling theory (MCT) of glassy dynamics [52] to systems of attractive colloids has been met by a considerable degree of success [20]. Recent studies [69], however, have shown that MCT predictions for systems associated with very small ranges of attraction wrongfully predicts structural arrest in the (metastable) single-phase fluid region at low colloid concentrations. In Paper IV we examine in greater detail how the attraction-driven glass transition behaves within MCT as the attraction range among colloids is shortened. The aim is ultimately to understand the tendency of MCT to overpredict structural arrest. This is done for a square-well interaction. We also develop some simplifications of the theory.

The dynamic structure factor $S(q,t)$ can be measured by dynamic light or X-ray scattering. For gels and glasses $S(q,t)$ does not decay completely with time. The remainder is related to the so-called non-ergodicity factor $f(q) = \lim_{t\to\infty} S(q,t)/S(q)$. MCT provides a closed equation for this quantity (equation 5.27), which can be solved if a static structure factor $S(q)$ or direct correlation function $c(q) = (S(q)-1)/nS(q)$ is known, usually from some approximate theory. For short-range attractions it is known that solutions for $f(q)$ are dominated by large wavevectors [18, 19, 70]. Two approximations can be made. The direct correlation function can be expressed as

$$c(q) = (A\cos q - B\cos q\lambda)/q^2 \tag{6.1}$$

where $A = 4\pi g(\sigma+)$ and $B = 4\pi g(\lambda\sigma+)\left(e^{\beta\epsilon}-1\right)$, and all the structure factors in equation 5.27 can be set equal to unity. In addition, from MC simulations of square-well fluids one sees that the radial distribution function inside the well width of the square-well interaction does not vary so much so that $|\frac{g(\lambda\sigma-)-g(\sigma+)}{g(\sigma+)}| \ll 1$. In this case it is possible to reduce the MCT

equation to a one-parameter model in terms of

$$\Gamma = \frac{6\phi_c\delta}{\pi^2} g(\sigma+)^2 \left(1 - e^{-\beta\epsilon}\right) \tag{6.2}$$

where the parameter Γ characterizes how strongly coupled the system is. Above a certain value, $\Gamma = 0.721$, $f(q)$ becomes non-zero, which means that MCT predicts structural arrest. In other words, to evaluate whether the theory predicts an arrest transition it is just necessary to compute the contact value of the radial distribution function and to compare the result of the right-hand side of equation 6.2 with the critical Γ value. One can use PY theory to accomplish this or one can use MC simulations. In figure 6.7 both MC simulations and PY theory have been used for a system with a 5% well width. In addition, an estimate of the critical point has been given, using a relation suggested by Noro and Frenkel [15]. The simple formula in equation 6.2 has been verified in Paper IV to reproduce the predictions of the full MCT up to ϕ_c of about 0.5 for sufficiently short-range square-well interactions. In figure 6.7 most points shown would probably correspond to fluid-crystal coexistence if the system had been allowed to reach equilibrium. In this case the systems were instantaneously brought from fluid points at $\epsilon/(k_BT) = 1.5$ to the points shown. After an initial, rapid change in the structure a metastable radial distribution function could usually be extracted as also shown in figure 6.7. As also seen, it does not matter too much whether MC simulations or PY theory is used. In both cases MCT predicts structural arrest well on the fluid side of the critical point.

It is instructive to examine the MCT predictions (using PY theory for $g(\sigma+)$) as the well width is decreased further, and how it compares to the critical point and the fluid-crystal freezing transition. In figure 6.8 this is done for a volume fraction of 0.15 and $\tau^{-1} = (12\delta e^{\beta\epsilon})$ which is related to the second virial coefficient. For larger well widths there are MC simulation results available [64, 71–74], which suggest that the critical point approaches a constant τ value equal to that found by Miller and Frenkel for the so-called Baxter limit [45, 76]. In contrast, the MCT prediction for arrest approaches incorrectly higher τ as δ is decreased. The same, however, seems to be the case for the freezing transition. This suggest that the type of transition that MCT predicts for very short ranges of attraction is more related to crystallization than fluid-fluid phase separation. Indeed similarities have been noted between the structure of the MCT equations and theories used to predict crystallization [77]. Gels, however, are typically found in the vicinity of fluid-fluid transitions, and it seems clear that MCT is not capable of describing gel formation for systems with very short-range attractions.

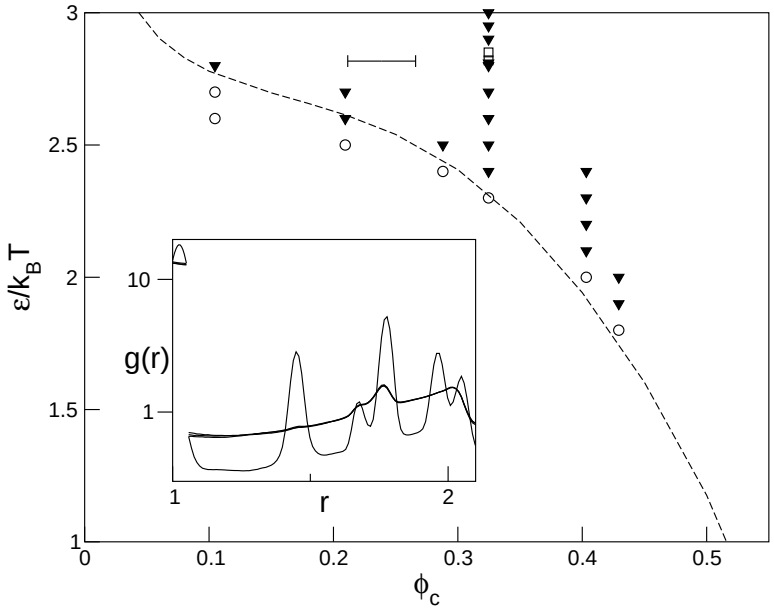

Figure 6.7: Phase diagram showing MCT predictions based on results from Monte Carlo simulations for $g(\sigma+)$ and $g(\lambda\sigma+)$ in terms of scaled well depth and volume fraction for a square-well system with $\lambda = 1.05$. The equilibrium fluid-crystal phase boundary is not shown. Open circles and inverted triangles, represent ergodic fluid and nonergodic states, respectively. The critical point estimate is shown by the horizontal error bar. The system shown by the open square crystallized too rapidly for evaluation of a liquid-like $g(r)$. The inset shows $g(r)$ at $\phi_c = 0.325$ for $\epsilon/k_BT = 2.85$ (crystalline), $2.9, 2.95$, and 3.0. The dashed line represent results based on PY input.

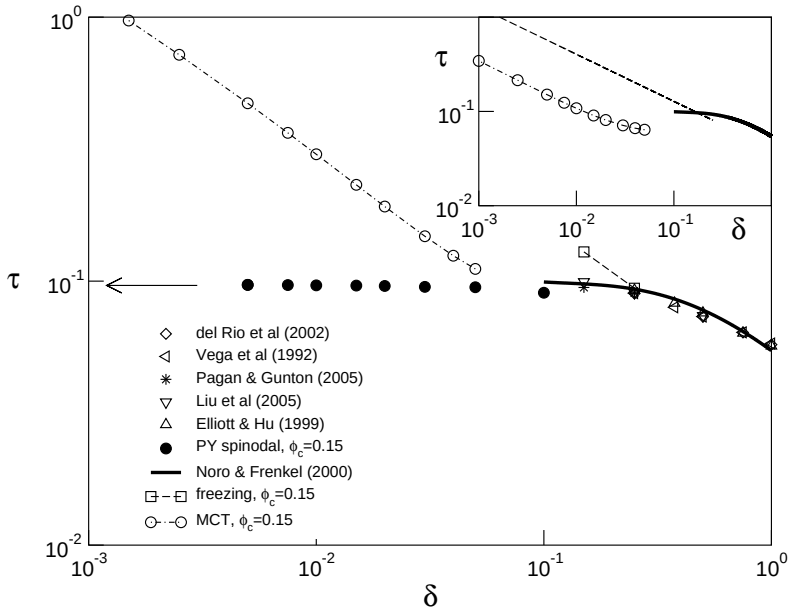

Figure 6.8: Phase diagram in terms of $\tau = (12\delta e^{\beta\epsilon})^{-1}$ as a function of the square-well range of attraction. Computer simulation estimates [64, 71–74] of the critical point are shown as symbols along with the corresponding state predictions of Noro and Frenkel [15], as labeled. The compressibility estimate for the spinodal at $\phi_c = 0.15$ from Percus-Yevick theory is shown as filled circles, with the arrow pointing to the corresponding Baxter result [45]. The squares are freezing point estimates at $\phi_c = 0.15$, interpolated from computer simulation data [71]. The inset shows the Noro-Frenkel prediction for the critical point together with an estimate of the freezing transition [75] and MCT transition at $\phi_c = 0.02$.

Chapter 7

Conclusions and future outlook

Computer simulations are an important tool in research, particularly for investigating systems that are difficult to study and for which properties are difficult to interpret. Colloidal particles with short-range attractions fall in this category. It is difficult experimentally to determine the phase behavior when multiple phases coexist and combine with non-equilibrium processes, like gelation and glass transitions. In this thesis aim was taken at staying close to the experimental systems but at the same time without overly complicating matters. The one-component AO potential was selected for most of this work but a two-component AO model was considered in Paper I to make sure many-body contributions were small. In this context, it was shown that insertions formulas can be derived which allow for Monte Carlo determinations of radial distribution functions and some approximate theories were suggested and tested. Polydispersity, which is almost always an issue experimentally, was considered in Paper II and the effects it has on phase behavior. Also, the Gibbs ensemble method was applied in a novel way to speed up equilibration of two-phase systems that would otherwise get stuck on their way to equilibrium. Rather than using molecular dynamics, a Brownian dynamics algorithm more appropriate for colloidal particles was tested and used in Paper III in which the dynamics was followed. Even though the dynamics was slowed down for high particle and polymer concentrations, no structural arrest could be identified, perhaps because it requires even higher stronger attractions. The predictions of MCT were compared in Paper I for intermediate-range attractions and was seen to qualitatively match the region where gels are found. For very short-range attractions the theory predicts such transitions in the fluid-phase region where none are found experimentally. In Paper IV MCT predictions were shown to follow the fluid-crystal freezing transition instead of the fluid-fluid critical point, which shows that the theory is not appropriate for such short-range attractive systems.

There are several issues that have come up during this work that warrant further study and some examples are given here. In Paper II it was found that direct application of GEMC simulations to AO systems with a small polymer-colloid size ratio, i.e. systems characterized by a short-range attractions, got stuck on the way towards equilibrium. Since only 500 particles were used, the scale of the structures formed in these stuck configurations were small, but they are nevertheless reminiscent of microscopy images of actual colloidal gels with connected particle clusters and voids [23, 78]. Therefore, it should be of interest to conduct GEMC simulations of considerably larger systems in the same way to examine the types of structures generated and how they compare with microscopy data.

Obtaining fully equilibrated phase equilibria data for short-range attractive systems is an obvious target for future study. The sequential equilibration scheme suggested in Paper II begins to break down at AO attraction ranges of about 10% of the mean particle diameter. The method is in many ways a manual way of conducting so-called parallel tempering. It is most similar to the parallel tempering method developed by Bunker and Dünweg [79] in which they allow for Monte Carlo exchanges of configurations between systems, simulated in parallel, characterized by different values for the parameters of the interaction potential. This parallel tempering method was tested briefly but all the configurational exchanges between systems with small values of the size ratio were rejected in applying the Monte Carlo acceptance criterion. Perhaps a better way can be found to choose the potential parameters for the different systems, making exchange of configurations more likely.

Although the dynamics, as found by BD simulation, slows down as one increases the polymer concentration, no clear signs of structural arrest were observed. This is in contrast to experiments [22] in which structural arrest is found at what should be comparable polymer concentrations and ranges of attraction. One could follow what has been done using molecular dynamics simulations [80, 81] and examine the dynamics for even stronger attractions using higher polymer concentrations. Since, according to Paper II, particles do not exchange between phases in the GEMC simulations, it may be that structural arrest is facilitated by introducing regions of dilute fluid (essentially voids) in the dense-fluid structure, in effect introducing the interface between phases that is removed in GEMC method. This could be done by diluting the dense fluids studied in Paper III. It would then also be of interest to compare structures obtained by the usual path of raising the polymer concentration at constant volume fraction of colloidal particles.

Acknowledgments

To my supervisor Johan Bergenholtz, for accepting me in your group and providing me with an interesting project. Your door has always been open and you have always been willing to share your great knowledge. It has been a pleasure to work with you. Thank you!

To the members of the Physical Chemistry group, both former and present, for making my time in the group enjoyable. We have spent many lunches together, always finding something interesting to discuss. I wish you all good luck in the future!

Fredrik, älskade du..... Tack för allt!

,

Bibliography

[1] P. C. Zamora D. Rosenbaum and C. F. Zukoski. Phase behavior of small attractive colloidal particles. *Phys. Rev. Lett.*, 76:150–153, 1996.

[2] E. Zaccarelli. Colloidal gels: equilibrium and non-equilibrium routes. *J. Phys.: Condens. Matter*, 19:323101, 2007.

[3] S. Asakura and F. Oosawa. On interaction between two bodies immersed in a solution of macromolecules. *J. Chem. Phys.*, 22:1255, 1954.

[4] S. Asakura and F. Oosawa. Interactions between particles suspended in solutions of macromolecules. *J. Polym. Sci.*, 33:183, 1958.

[5] A. Vrij. Polymers at interfaces and the interactions in colloidal dispersions. *Pure & Appl. Chem.*, 48:471–483, 1976.

[6] M. D. Haw. Colloidal suspensions, Brownian motion, molecular reality: a short history. *J. Phys.: Condens. Matter*, 14:7769–7779, 2002.

[7] W. C. K. Poon. The physics of a model colloid-polymer mixture. *J. Phys.: Condens. Matter*, 14:R859, 2002.

[8] P. N. Pusey and W. van Megen. Phase-behavior of concentrated suspensions of nearly hard colloidal spheres. *Nature (London)*, 320:340, 1986.

[9] W. G. Hoover and F. H. Ree. . *J. Chem. Phys.*, 49:3609–3617, 1968.

[10] W. van Megen and P. N. Pusey. Dynamic light-scattering study of the glass transition in a colloidal suspension. *Phys. Rev. A*, 43:5429, 1991.

[11] W. Götze and L. Sjögren. Beta–relaxation at the glass–transition of hard–spherical colloids. *Phys. Rev. A*, 43:5442, 1991.

[12] A. P. Gast, C. K. Hall, and W. B. Russel. Polymer induced phase separations in non–aqueous colloidal suspensions. *J. Colloid Interf. Sci.*, 96:251, 1983.

[13] H. N. W. Lekkerkerker, W. C. K. Poon, P. N. Pusey, A. Stroobants, and P. B. Warren. Phase behaviour of colloid + polymer mixtures. *Europhys. Lett.*, 20:559, 1992.

[14] H. N. W. Lekkerkerker C. F. Tejero, A. Daanoun. Phase-diagrams of simple fluids with extreme pair potentials. *Phys. Rev. Lett.*, 73:752–755, 1994.

[15] M. G. Noro and D. Frenkel. Extended corresponding-states behavior for particles with variable range attractions. *J. Chem. Phys.*, 113:2941, 2000.

[16] P. Bolhuis and D. Frenkel. Prediction of an expanded-to-condensed transition in colloidal crystals. *Phys. Rev. Lett.*, 72:2211–2214, 1994.

[17] F. Sciortino. Disordered materials – One liquid, two glasses. *Nature (London).*

[18] J. Bergenholtz and M. Fuchs. Nonergodicity transitions in colloidal suspensions with attractive interactions. *Phys. Rev. E*, 59:5706, 1999.

[19] L. Fabbian, W. Götze, F. Sciortino, P. Tartaglia, and F. Thiery. Ideal glass–glass transitions and logarithmic decay of correlations in a simple system. *Phys. Rev. E*, 59:R1347, 1999.

[20] K. Pham, A. M. Puertas, J. Bergenholtz, S. U. Egelhaaf, A. Moussaïd, P. N. Pusey, A. B. Schofield, M. E. Cates, M. Fuchs, and W. C. K. Poon. Multiple glassy states in a simple model system. *Science*, 296:104, 2002.

[21] T. Eckert and E. Bartsch. Re-entrant glass transition in a colloid-polymer mixture with depletion attractions. *Phys. Rev. Lett.*, 89:125701, 2002.

[22] S. M. Ilett, A. Orrock, W. C. K. Poon, and P. N. Pusey. Phase behavior of a model colloid–polymer mixture. *Phys. Rev. E*, 51:1344, 1995.

[23] P. J. Lu, E. Zaccarelli F. Ciulla, A. B. Schofield, F. Sciortino, and D. A. Weitz. Gelation of particles with short-range attraction. *Nature (London)*, 453:499, 2008.

[24] J. M. Brader, M. Dijkstra, and R. Evans. Inhomogeneous model colloid–polymer mixtures: Adsorption at a hard wall. *Phys. Rev. E*, 63:041405, 2001.

[25] R. Roth and R. Evans. The depletion potential in non-additive hard-sphere mixtures. *Europhys. Lett.*, 53:271, 2001.

[26] J. M. Mendez-Alcaraz and R. Klein. Depletion forces in colloidal mixtures. *Phys. Rev. E.*

[27] G. V. Schulz. . *Z. Phys. Chem. Abt. B*, 43:25, 1939.

[28] B. H. Zimm. . *J. Chem. Phys.*, 16:1099, 1948.

[29] B. D'Aguann and R. Klein. Integral-equation theory of polydisperse Yukawa systems. *Phys. Rev. A*, 46:7652, 1992.

[30] D. Frenkel and B. Smit. *Understanding Molecular Simulation.* Academic Press, San Diego, 2002.

[31] M. N. Rosenbluth A.N. Teller N. Metropolis, A. W. Rosenbluth and E. Teller. Equation of state calculations by fast computing machines. *J. Chem. Phys.*, 21:1087–1092, 1953.

[32] Panagiotopoulos. Direct determination of phase coexistence properties of fluids by Monte Carlo simulations in a new ensemble. *Molec. Phys*, 61:813–826, 1987.

[33] B. Smit and D. Frenkel. Calculation of the chemical potential in the Gibbs ensemble. *Molec. Phys*, 68:951, 1989.

[34] D. L. Ermak. A computer simulation of charged particles in solution. I. technique and equilibrium properties. *J. Chem. Phys.*, 62:4189, 1975.

[35] J. D. Doll P. J. Rossky and H. L. Friedman. Brownian dynamics as smart monte carlo simulation. *J. Chem. Phys.*, 69:4628, 1978.

[36] M. H. Kalos D. Ceperley and J. L. Lebowitz. *Macromolecules*, 14:1472, 1981.

[37] D. M. Heyes and A. C. Branka. Monte carlo as brownian dynamics. *Molec. Phys*, 94:447, 1998.

[38] B. Cichocki and K. Hinsen. Dynamic computer simulation of concentrated hard sphere suspensions. *Physica A*, 166:473, 1990.

[39]

[40] D. E. Knuth. *The art of computer programming.* Addison-Wesley, Reading, MA, 1998.

[41] P. Turq M. Jardat, O. Bernard and G. R. Kneller. *J. Chem. Phys.*, 110:7993, 1999.

[42] J. P. Hansen and I. R. McDonald. *Theory of Simple Liquids*. Academic Press, London, 1986.

[43] M. S. Wertheim. The exact solution of Percus-Yevick integral equation for hard spheres. *Phys. Rev. Lett.*, 10:321, 1963.

[44] E. Thiele. Equation of state for hard spheres. *J. Chem. Phys.*, 39:474, 1963.

[45] R. J. Baxter. Percus-Yevick equation for hard spheres with surface adhesion. *J. Chem. Phys.*, 49:2770, 1968.

[46] B. Widom. Some topics in the theory of fluids. *J. Chem. Phys.*, 39:2808, 1963.

[47] T. Boublik. Hard-sphere equation of state. *J. Chem. Phys.*, 53:471, 1970.

[48] N. F. Carnahan G. A. Mansoori and K. E. Starling. Equilibrium thermodynamic properties of mixture of hard sphers. *J. Chem. Phys.*, 54:1523, 1971.

[49] J. J. Salacuse and G. Stell. Polydisperse systems – statistical thermodynamics, with applications to several models including hard and permeable spheres. *J. Chem. Phys.*, 77:3714–3725, 1982.

[50] E. Helfand J. L. Lebowitz and E. Praestga. Scaled particle theory of fluid mixtures. *J. Chem. Phys.*, 43:774, 1965.

[51] W. Götze and L. Sjögren. *Rep. Prog. Phys.*, 55:241, 1992.

[52] U. Bengtzelius, W. Götze, and A. Sjölander. *J. Phys. C*, 17:5915, 1984.

[53] E. Zaccarelli, G. Foffi, F. Sciortino, P. Tartaglia, and K. A. Dawson. Gaussian density fluctuations and mode coupling theory for supercooled liquids. *Europhys. Lett.*, 55:157, 2001.

[54] G. Szamel and H. Löwen. Mode-coupling theory of the glass transition in colloidal systems. *Phys. Rev. A*, 44:8215, 1991.

[55] J. K. G. Dhont. *An introduction to dynamics of colloids*. Elsevier, Amsterdam, 1996.

[56] W. Götze and L. Sjögren. General properties of certain non-linear integro-differential equations. *J. Math. Anal. Appl.*, 195:230, 1995.

[57] B. O'Malley and I. Snook. Structure of hard-sphere fluid and precursor structures to crystallization. *J. Chem. Phys.*, 123:054511, 2005.

[58] P. B. Warren, S. M. Ilett, and W. C. K. Poon. Effect of polymer non-ideality in a colloid–polymer mixture. *Phys. Rev. E*, 52:5205, 1995.

[59] P. N. Pusey and W. van Megen. Observation of a glass transition in suspensions of spherical colloidal particles. *Phys. Rev. Lett.*, 59:2083, 1987.

[60] W. van Megen and S. M. Underwood. Glass transition in colloidal hard spheres: measurement and mode-coupling-theory analysis of the coherent intermediate scattering function. *Phys. Rev. E*, 49:4206, 1994.

[61] A. P. Gast, W. B. Russel, and C. K. Hall. An experimental and theoretical study of phase transitions in the polystyrene latex and hydroxyethylcellulose system. *J. Colloid Interf. Sci.*, 109:161, 1986.

[62] J. Pande et al. M.L. Broide, C. R. Berland. Binary-liquid phase-separation of lens protein solutions.

[63] F. Rosenberger M. Muschol. Liquid-liquid phase-separation in supersaturated lysozyme solutions and associated precipitate formation/crystallization. *J. Chem. Phys.*, 107:1953–1962, 1997.

[64] D. L. Pagan and J. D. Gunton. Phase behavior of short-range square-well model. *J. Chem. Phys.*, 122:184515, 2005.

[65] D. G. Green, G. Jackson, E. de Miguel, and L. F. Rull. Vapor-liquid and liquid-liquid phase equilibria of mixtures containing square-well molecules by Gibbs ensemble Monte Carlo simulation. *J. Chem. Phys.*, 101:3190, 1994.

[66] A. Einstein. *Investigations on the theory of Brownian movement.* Dover, New York, 1956.

[67] W. Kob, C. Donati, S. J. Plimpton, P. H. Poole, and S. C. Glotzer. Dynamical heterogeneities in a supercooled Lennard-Jones liquid. *Phys. Rev. Lett.*, 79:2827, 1997.

[68] E. Weeks, J. C. Crocker, A. C. Levitt, A. Schofield, and D. A. Weitz. Three-dimensional direct imaging of structural relaxation near the colloidal glass transition. *Science*, 287:627, 2000.

[69] G. Foffi, C. De Michele, F. Sciortino, and P. Tartaglia. Scaling of dynamics with the range of interaction in short-range attractive colloids . *Phys. Rev. Lett.*, 94:078301, 2005.

[70] K. A. Dawson, G. Foffi, M. Fuchs, W. Götze, F. Sciortino, M. Sperl, P. Tartaglia, Th. Voigtmann, and E. Zaccarelli. Higher–order glass–transition singularities in colloidal systems with attractive interactions. *Phys. Rev. E*, 63:011401, 2000.

[71] H. Liu, S. Garde, and S. Kumar. Direct determination of phase behavior of square-well fluids. *J. Chem. Phys.*, 123:174505, 2005.

[72] L. Vega, E. de Miguel, L. F. Rull, G. Jackson, and I. A. McLure. Phase equilibria and critical behavior of square-well fluids of variable width by Gibbs ensemble Monte Carlo simulation. *J. Chem. Phys.*, 96:2296, 1992.

[73] J. R. Elliott and L. G. Hu. Vapor-liquid equilibria of square-well spheres. *J. Chem. Phys.*, 110:3043, 1999.

[74] F. del Rio, E. Avalos, R. Espindola, L. F. Rull, G. Jackson, and S. Lago. Vapour-liquid equilibrium of the square-well fluid of variable range via a hybrid simulation approach. *Molec. Phys*, 100:2531, 2002.

[75] P. Charbonneau and D. Frenkel. Gas-solid coexistence of adhesive spheres. *J. Chem. Phys.*, 126:196101, 2007.

[76] M. A. Miller and D. Frenkel. Phase diagram of the adhesive hard sphere fluid. *J. Chem. Phys.*, 121:535, 2004.

[77] T. R. Kirkpatrick and P. G. Wolynes. . *Phys. Rev. A*, 35:3072, 1987.

[78] M. J. Solomon P. Varadan. Direct visualization of long-range heterogeneous structure in dense colloidal gels. *Langmuir*, 19:509–512, 2003.

[79] B. Dunweg A. Bunker. Parallel excluded volume tempering for polymer melts. *Phys. Rev. E*, 63, 2001.

[80] M. E. Cates A. M. Puertas, M. Fuchs. Mode coupling and dynamical heterogeneity in colloidal gelation: A simulation study.

[81] M. E. Cates A. M. Puertas, M. Fuchs. Competition between glass transition and liquid-gas separation in attracting colloids. *J. Phys.: Condens. Matter*, 19, 2007.